Joint Active and Passive Beamforming for Vehicle Localization with Reconfigurable Intelligent Surfaces

Zhiyuan Feng, Bo Wang, *Member, IEEE*, Zheng Chang, *Senior Member, IEEE*, Timo Hämäläinen, *Senior Member, IEEE*, Yanping Zhao and Fengye Hu, *Senior Member, IEEE*

***Abstract*—Future vehicle localization will be committed to improving the positioning accuracy and energy efficiency of localization systems in the intelligent transportation. Recently, reconfigurable intelligent surface (RIS) as an emerging technology has gained widespread attention and is favorable to enhance the performance of vehicle localization systems because of its capacity of customizing the wireless channel. In this paper, in order to minimize the transmit power, we consider the joint active and passive beamforming problem of RIS-assisted vehicle localization system under the constraints of the localization accuracy and the phase shift parameters of the RIS. Specifically, we establish the model of RIS-assisted vehicle localization system and derive the Cramér-Rao bound (CRB) as the localization performance metric. Next, for the scenario of single vehicle localization, we derive the optimal RISs' phases, and obtain the optimal solution for joint active and passive beamforming based on semidefinite programming relaxation of the non-convex beamforming problem and the corresponding equivalent analysis. Lastly, aimming to the scenario of multiple vehicles localization, we transform the nonconvex joint active and passive beamforming problem into semidefinite programming (SDP) and geometric programming (GP) form subproblems through alternating optimization. Simulation results verify the feasibility of the proposed methods.**

***Index Terms*—Reconfigurable intelligent surface, vehicle localization, joint active and passive beamforming, Cramér-Rao bound, convex optimization.**

I. Introduction

VEHICLE localization is an important topic in wireless network research and intelligent transportation system [1]–[5]. The range-based localization through capturing the distance and angle parameters is a common technology for urban vehicle localization [6]–[10]. Generally, the range metrics for localization include time of arrival (TOA), time difference of arrival (TDOA) and angle of arrival (AOA), etc [11]–[13]. In order to improve the localization accuracy, [14] obtains the closed form results of target localization by using the weighted least squares method. [15] brings quadratic constraints to solve the problem of decreased localization accuracy in high noise scenarios. In addition, by combining two or more range metrics, an accurate estimation of the vehicle position or velocity can be achieved.

Although the vehicle localization technologies mentioned above can meet basic localization needs, these methods are only used in the scenario where the line of sight (LOS) link exists. Once the LOS link between the transmitter or receiver and the vehicles is obstructed, the range-based localization methods will be difficult to capture accurate range measurements, and the position of the vehicle will become hard to estimate. Recently, Reconfigurable Intelligent Surface (RIS) [16]–[20] has gained widespread attention due to its advantage of being able to customize wireless channels by adjusting phase shift parameters. In other words, RIS can establish a virtual line of sight (VLOS) to overcome non-line of sight (NLOS) problems. For example, [21] proposes the design method of time-varying reflection coefficient for RIS under NLOS. [22] utilizes RIS components for joint localization and environmental sensing in the NLOS millimeter-wave (mmWave) communication system. In addition, RIS can not only address NLOS issues, but also help improve communication and localization quality. [23] conducts an investigation into the near-field localization system assisted by RIS, while the beamforming design scheme of the RIS-assisted integrated sensing and communication is discussed in [24]. [25] proposes an iterative and incremental joint multi-user communication and environment sensing scheme based on RIS. [26] and [27] use statistical channel state information to discuss the performance gain of RIS in communication system. These works show that introducing RIS into intelligent transportation system to assist vehicle localization is a reasonable and promising direction. Particularly, the beamforming design of transmitter and the phase optimization of RIS are crucial for reducing the energy consumption of localization systems.

In recent years, the beamforming problems [28]–[32] are extensively investigated in the fields of communication, detection, and localization. Beamforming can make the radiation pattern of antenna array adapt to a specific target direction, which improve the efficiency and reduce the energy consumption to a certain extent. For instance, [31] proposes a

This work was supported in part by the National Natural Science Foundation of China under Grant 61771217 and Grant 62071105, in part by the Funds for International Cooperation and Exchange of the National Natural Science Foundation of China under Grant 62111530072, in part by the Natural Science Foundation of Jilin Province under Grant 20220101099JC, and in part by the Chinese Scholarship Council (CSC).(Corresponding author: Bo Wang.)

Zhiyuan Feng, Bo Wang, Yanping Zhao and Fengye Hu are with the College of Communication Engineering, Jilin University, Changchun 130012, China (e-mail: zyfeng21@mails.jlu.edu.cn; roywang@jlu.edu.cn; zhaoyp@jlu.edu.cn; hufy@jlu.edu.cn).

Zheng Chang is with the School of Computer Science and Engineering, University of Electronic Science and Technology of China, Chengdu 611731, China, and also with the Faculty of Information Technology, University of Jyväskylä, 40014 Jyväskylä, Finland (e-mail: zheng.chang@jyu.fi).

Timo Hämäläinen is with the Faculty of Information Technology, University of Jyväskylä, 40014 Jyväskylä, Finland (e-mail: timo.t.hamalainen@jyu.fi).

robust digital beamforming technique based on interference plus noise covariance matrix reconstruction. [32] investigates the joint transmit beamforming problem of MIMO radar and multiple user MIMO communication. The above research is mainly about the active beamforming, while the RIS, as a passive component, can also enable the beam to point toward the target direction by passive beamforming. As a result, the joint active and passive beamforming design of transmitter and RIS is a worthwhile research topic.

However, most of the literature on beamforming focuses on the communication and localization research of traditional systems without RIS. In [33], the authors consider the joint active and passive beamforming problem for RIS-assisted radar surveillance with the goal of maximizing the target illumination power. On the contrary, this paper concentrates on the joint active and passive beamforming of the RIS-assisted vehicle localization system, and utilizes the Cramér-Rao bound (CRB) as the optimization criterion, which is the explicit expression of the localization performance. In addition, two RISs are respectively deployed in the near field range of the transmitter and receiver, which can provide a larger performance gain than the far field scenario and also leads to a more complex system model [34]–[37]. Therefore, the beamforming problem of RIS-assisted vehicle localization system based on CRB and the near field model is more complex than the other. In this paper, we investigate the joint active and passive beamforming problems for two scenarios. Specifically, we first of all derive the CRB of vehicle localization assisted by RIS as the performance metric, and present the joint active and passive beamforming results of single vehicle scenario by using the specialized CRB. Subsequently, for the multiple vehicles scenario, we decompose the original non-convex optimal problem into two subproblems, and obtain the semidefinite programming (SDP) form using convex release to solve the passive beamforming problem. On this basis, the active beamforming problem is transformed into a geometric programming (GP) problem.

The major contributions of this paper are summarized below.

- Firstly, we provide the RIS-assisted vehicle localization model and derive the CRB as performance threshold measure for vehicle position parameters. Then, we formulate a joint active and passive beamforming problem with the goal of minimizing total transmit power under the constraints of localization accuracy and RISs' phases.
- Secondly, we propose single vehicle beamforming optimization (SVBO) method to solve the beamforming optimization problem in this context. The optimal results of passive beamforming optimization are obtained by utilizing the characteristic of maximum pointing gain in the beamforming pattern. Then, we transform the localization performance constraint CRB into a closed form expression, and release the active beamforming problem as a SDP problem. Furthermore, we prove that the SDP problem is equivalent to the original active beamforming problem to ensure that the released problem has the same optimal solution as the original problem.
- Finally, we propose multiple vehicles beamforming algorithm (MVBA) in regard to multiple vehicles localization. By using alternating optimization techniques, the original problem is split into two subproblems, i.e., the optimization problems of RIS near the transmitter and receiver, respectively. The passive beamforming problem is released as a feasibility problem in SDP form, while the active beamforming problem is solved as a GP problem through equivalent change and perspective function.

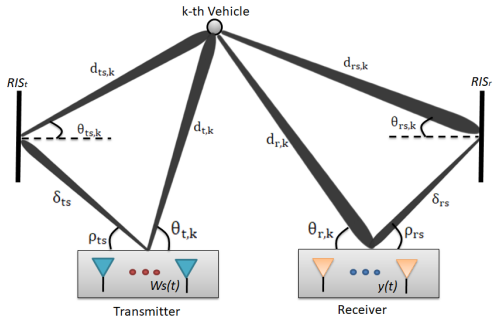

Fig. 1. Structure diagram of vehicle localization with RISs-assisted configuration.

The outline of this paper is organized as follows. In Section II, the RIS-assisted vehicle localization model and beamforming problem are elaborated. In Section III, we derive CRB as a localization performance metric in detail. Section IV proposes SVBO method to solve the beamforming problem in single vehicle scenario. Section V addresses the beamforming problem in multiple vehicles scenario. Simulation examples are presented in Section VI. Conclusions are drawn in Section VII.

Notation: Throughout this paper, we use $(.)^T$, $(.)^*$ and $(.)^H$ denote the transpose, complex conjugate, and complex conjugate transpose, respectively. $\mathbb{R}^+$ stands for the set of positive real numbers, while $\mathbb{R}^{i\times j}$ and $\mathbb{C}^{i\times j}$ represent the sets of real and complex matrix with i rows and j columns, separately. Lowercase, bold lowercase, and bold uppercase letters are used for scalar variable, vector, and matrix, respectively. (a, b) denotes the open interval from a to b. $[.]_{i,j}$ is the ith row and jth column entry of matrix. $tr(.)$, $diag(.)$, $(.)^{-1}$, $\|.\|_2$, $|.|$, $(.)'$ and $E[.]$ stand for the trace operator, diagonal operator, inverse operator, Euclidean norm, modulus operator, derivative and expectation, respectively, while matrix $\boldsymbol{A} \succeq \boldsymbol{B}$ means that $\boldsymbol{A} - \boldsymbol{B}$ is positive semidefinite.

II. PROBLEM FORMULATION

A. System Model

We consider a RIS-assisted MIMO radar system for vehicle localization shown in Fig. 1. The radar transmitter and receiver at different locations are equipped with N_t and N_r densely spaced elements respectively arranged in a uniform linear array (ULA) with emitting N_t orthogonal waveforms of equal power from each radiating element. This model is assumed to be in a two-dimensional scenario, where the two RISs are vertically arranged. This model is easily extended to three-dimensional scenario in localization algorithms [38], [39]. The

two identical RIS (which are represented as $\mathbf{RIS}_t$ and $\mathbf{RIS}_r$) are deployed in the near field region of the transmitter and receiver respectively to assist the transmitter to illuminate the intended vehicle and to help the receiver capture the power scattered by the vehicle. The two surfaces are composed of N_{ts} and N_{rs} elements and can change their phases to establish a virtual data link between the array units and each RIS.

Let coordinate parameters of transmitter and receiver be $\boldsymbol{p}_t = [p_{tx}, p_{ty}]^T$ and $\boldsymbol{p}_r = [p_{rx}, p_{ry}]^T$, respectively. Suppose that the position parameters of the center elements of RISs are $\boldsymbol{p}_{ts} = [p_{tsx}, p_{tsy}]^T$ and $\boldsymbol{p}_{rs} = [p_{rsx}, p_{rsy}]^T$ as the reference points. It is worth emphasizing that the two RISs are deployed in the near field region of the radar transmitter and receiver respectively [34]–[37], while the vehicle of interest is in the far field region of the radar transmitter and receiver for meeting a larger localization range. The vehicle system assisted by RISs is used to locate K vehicles, where $\boldsymbol{p}_{m,k} = [p_{mx,k}, p_{my,k}]^T$ represents the position of the vehicle k being located. Let $\boldsymbol{s}(t) = [s_1(t), s_2(t), \cdots, s_K(t)]^T$ be a $K \times 1$ vector of orthogonal transmitted signal (such as beat frequency division (BFD) method), which satisfies $\int \boldsymbol{s}(t)\boldsymbol{s}^H(t) = \boldsymbol{I}_K$, where $\boldsymbol{I}_K$ represents the identity matrix of size N. We let $s_k(t), k = 1, 2, \cdots, K$, be the transmitted signal to the vehicle k and integrate a corresponding matrix $\boldsymbol{W} \in \mathbb{C}^{N_t \times K}$ as the beamforming matrix of the transmitter. As a result, the output signal of the transmitter is defined as $\boldsymbol{W}\boldsymbol{s}(t)$. We assume that the signals of each vehicle are separable at the receiver based on their distance, then the signal $\boldsymbol{y}_k(t) \in \mathbb{C}^{N_r \times 1}$ received by the receiver can be expressed as

$$\boldsymbol{y}_k(t) = \boldsymbol{H}_k \boldsymbol{W}\boldsymbol{s}(t) + \boldsymbol{n}_k(t), k = 1, 2, \cdots, K, \tag{1}$$

where $\boldsymbol{H}_k \in \mathbb{C}^{N_r \times N_t}$ is the channel parameter for vehicle k, and $\boldsymbol{n}_k(t)$ denotes a Gaussian vector with covariance matrix $\sigma^2\boldsymbol{I}$, accounting for the additive noise. The channel $\boldsymbol{H}_k$ takes on a more complex form due to the existence of RIS. The MIMO radar utilizes echoes for localization and the signal goes through the four channels: "Transmitter - Vehicle - Receiver", "Transmitter - $\mathbf{RIS}_t$ - Vehicle - Receiver", "Transmitter - Vehicle - $\mathbf{RIS}_r$ - Receiver", and "Transmitter - $\mathbf{RIS}_t$ - Vehicle - $\mathbf{RIS}_r$ - Receiver". Therefore, the channel $\boldsymbol{H}_k$ can be written in (2). Where $\gamma_{t,k}$ and $\gamma_{r,k}$ denote the direct channels between the reference transmit element and the vehicle and between the vehicle and the reference receive element for vehicle k, respectively. $\gamma_{ts,k}$ and $\gamma_{rs,k}$ are the two-hop indirect channels from the reference transmit element to the reference forward reflecting element to the vehicle and from the vehicle to the reference backward reflecting element to the reference receive element for vehicle k, respectively. According to the standard radar equation, the scalar channels $\gamma_{t,k}$, $\gamma_{r,k}$, $\gamma_{ts,k}$ and $\gamma_{rs,k}$ can be modeled as [40], [41]

$$\gamma_{t,k} = \left(\frac{\kappa_{t,k}}{4\pi d_{t,k}^2}\right)^{1/2} e^{-j2\pi d_{t,k}/\lambda}, \tag{3a}$$

$$\gamma_{r,k} = \left(\frac{\kappa_{r,k}\lambda^2}{(4\pi)^2 d_{r,k}^2}\right)^{1/2} e^{-j2\pi d_{r,k}/\lambda}, \tag{3b}$$

$$\gamma_{ts,k} = \left(\frac{\kappa_{ts,k}\varsigma_{t,k}\left(\rho_{ts}, \theta_{ts,k}\right)}{(4\pi)^2 \delta_{ts}^2 d_{ts,k}^2}\right)^{1/2} e^{-j2\pi(\delta_{ts}+d_{ts,k})/\lambda}, \tag{3c}$$

$$\gamma_{rs,k} = \left(\frac{\kappa_{rs,k}\varsigma_{r,k}\left(\rho_{rs}, \theta_{rs,k}\right)\lambda^2}{(4\pi)^3 \delta_{rs}^2 d_{rs,k}^2}\right)^{1/2} e^{-j2\pi(\delta_{rs}+d_{rs,k})/\lambda}, \tag{3d}$$

where $\theta_{t,k}$, ρ_{ts} and $\theta_{ts,k}$ are the angles from the transmitter to the vehicle k, from the transmitter to $\mathbf{RIS}_t$, and from $\mathbf{RIS}_t$ to the vehicle k, respectively, while $\theta_{r,k}$, ρ_{rs} and $\theta_{rs,k}$ are the angles from the receiver to the vehicle k, from the receiver to $\mathbf{RIS}_r$, and from $\mathbf{RIS}_r$ to the vehicle k, respectively. $d_{t,k}$, δ_{ts} and $d_{ts,k}$ denote the distances from the transmitter to the vehicle k, from the transmitter to $\mathbf{RIS}_t$, and from $\mathbf{RIS}_t$ to the vehicle k, respectively. $d_{r,k}$, δ_{rs} and $d_{rs,k}$ represent the distances from the receiver to the vehicle k, from the receiver to $\mathbf{RIS}_r$, and from $\mathbf{RIS}_r$ to the vehicle k, respectively. $\kappa_{t,k}$, $\kappa_{r,k}$, $\kappa_{ts,k}$ and $\kappa_{rs,k}$ are the gains of the transmitter and receiver elements in the transmission direction for vehicle k, respectively. λ is the signal wavelength. $\varsigma_{t,k}\left(\rho_{ts}, \theta_{ts,k}\right)$ and $\varsigma_{r,k}\left(\rho_{rs}, \theta_{rs,k}\right)$ are the radar cross sections (RCSs) for vehicle k of the two RISs with respect to the angles of arrival (AOA) ρ_{ts}, $\theta_{rs,k}$ and angles of departure (AOD) $\theta_{ts,k}$, ρ_{rs}, respectively. Specifically, leveraging [42]–[45], the RCSs of two RISs can be defined as

$$\varsigma_{t,k}\left(\rho_{ts}, \theta_{ts,k}\right) = A[\cos(\rho_{ts})]^{\mathrm{q}}\left(4\pi A/\lambda^2\right)[\cos(\theta_{ts,k})]^{\mathrm{q}}, \tag{4a}$$

$$\varsigma_{r,k}\left(\rho_{rs}, \theta_{rs,k}\right) = A[\cos(\rho_{rs})]^{\mathrm{q}}\left(4\pi A/\lambda^2\right)[\cos(\theta_{rs,k})]^{\mathrm{q}}, \tag{4b}$$

where A is the area of the element, and q denotes the cosine exponent. $\boldsymbol{v}_{t,k}$ and $\boldsymbol{v}_{r,k}$ are the direct steering vectors of the transmitter and receiver towards the vehicle k, respectively. $\boldsymbol{v}_{ts,k}$ and $\boldsymbol{v}_{rs,k}$ are the steering vectors of the RISs near the transmitter and receiver towards the vehicle k, respectively. $\boldsymbol{G}_t$ and $\boldsymbol{G}_r$ are the normalized channel matrices between the transmitter and the near RIS and between the receiver and the near RIS, respectively. Specifically, $\boldsymbol{v}_{t,k}$, $\boldsymbol{v}_{r,k}$, $\boldsymbol{v}_{ts,k}$ and $\boldsymbol{v}_{rs,k}$ are direction vectors which are separately related to angles $\theta_{t,k}$, $\theta_{r,k}$, $\theta_{ts,k}$ and $\theta_{rs,k}$ with the following forms

$$\boldsymbol{v}_{t,k} = \left[1, e^{-j\frac{2\pi f_c d\sin\theta_{t,k}}{c}}, \cdots, e^{-j\frac{2\pi(N_t-1)f_c d\sin\theta_{t,k}}{c}}\right]^T, \tag{5a}$$

$$\boldsymbol{v}_{r,k} = \left[1, e^{-j\frac{2\pi f_c d\sin\theta_{r,k}}{c}}, \cdots, e^{-j\frac{2\pi(N_r-1)f_c d\sin\theta_{r,k}}{c}}\right]^T, \tag{5b}$$

$$\boldsymbol{v}_{ts,k} = \left[1, e^{-j\frac{2\pi f_c d\sin\theta_{ts,k}}{c}}, \cdots, e^{-j\frac{2\pi(N_{ts}-1)f_c d\sin\theta_{ts,k}}{c}}\right]^T, \tag{5c}$$

$$\boldsymbol{v}_{rs,k} = \left[1, e^{-j\frac{2\pi f_c d\sin\theta_{rs,k}}{c}}, \cdots, e^{-j\frac{2\pi(N_{rs}-1)f_c d\sin\theta_{rs,k}}{c}}\right]^T, \tag{5d}$$

$$\begin{aligned}\boldsymbol{H}_k &= (\boldsymbol{v}_{r,k}\gamma_{r,k})(\boldsymbol{v}_{t,k}\gamma_{t,k})^H + (\boldsymbol{v}_{r,k}\gamma_{r,k})(\boldsymbol{G}_t\boldsymbol{\Omega}_t\boldsymbol{v}_{ts,k}\gamma_{ts,k})^H + (\boldsymbol{G}_r\boldsymbol{\Omega}_r\boldsymbol{v}_{rs,k}\gamma_{rs,k})(\boldsymbol{v}_{t,k}\gamma_{t,k})^H + (\boldsymbol{G}_r\boldsymbol{\Omega}_r\boldsymbol{v}_{rs,k}\gamma_{rs,k})(\boldsymbol{G}_t\boldsymbol{\Omega}_t\boldsymbol{v}_{ts,k}\gamma_{ts,k})^H \\ &= (\boldsymbol{v}_{r,k}\gamma_{r,k} + \boldsymbol{G}_r\boldsymbol{\Omega}_r\boldsymbol{v}_{rs,k}\gamma_{rs,k})(\boldsymbol{v}_{t,k}\gamma_{t,k} + \boldsymbol{G}_t\boldsymbol{\Omega}_t\boldsymbol{v}_{ts,k}\gamma_{ts,k})^H,\end{aligned} \tag{2}$$

where f_c is the carrier frequency, d is the inter-element spacing of the RISs, c is the speed of light, and $j=\sqrt{-1}$ is the symbol for imaginary. The adjustable phase matrix $\boldsymbol{\Omega}_t$ and $\boldsymbol{\Omega}_r$ of the RISs can be expressed as

$$\boldsymbol{\Omega}_t = diag\left\{\vartheta_{t,1},\vartheta_{t,2},\ldots,\vartheta_{t,N_{ts}}\right\}\in\mathbb{C}^{N_{ts}\times N_{ts}}, \tag{6a}$$

$$\boldsymbol{\Omega}_r = diag\left\{\vartheta_{r,1},\vartheta_{r,2},\ldots,\vartheta_{r,N_{rs}}\right\}\in\mathbb{C}^{N_{rs}\times N_{rs}}. \tag{6b}$$

where $\vartheta_{t,i}=e^{j\phi_{t,i}}, i=1,2,\ldots,N_{ts}$ and $\vartheta_{r,i}=e^{j\phi_{r,i}}, i=1,2,\ldots,N_{rs}$. In order to extract effective localization information from the channel, we process the signal received by the receiver through a match filter. Then, the output of the received signal $\boldsymbol{y}_k$ can be represented as [46]

$$\begin{aligned}\boldsymbol{r}_k(\tau) &= \int_T \boldsymbol{y}_k(\tau-t)\,s_k^*(t)\,dt \\ &= \boldsymbol{H}_k\boldsymbol{\omega}_k + \int_T \boldsymbol{n}_k(\tau-t)\,s_k^*(t)\,dt.\end{aligned} \tag{7}$$

where $\boldsymbol{\omega}_k\in\mathbb{C}^{N_t\times 1}$ is the beamforming vector of vehicle k in the beamforming matrix $\boldsymbol{W}$. It is worth noting that the positions of the transmitter, receiver and nearby RIS are considered as the known parameters. Consequently, the related angles ρ_{ts}, ρ_{rs} and the distances δ_{ts}, δ_{rs} are also prescient parameters. Then, by using the sine and cosine of a triangle, the AOD $\theta_{ts,k}$, AOA $\theta_{rs,k}$ of RISs and the distance parameters $d_{ts,k}$, $d_{rs,k}$ can be respectively written as functions of the angles $\theta_{t,k}$, $\theta_{r,k}$ and the distances $d_{t,k}$, $d_{r,k}$, that is,

$$\theta_{ts,k} = \arctan\frac{d_{t,k}\sin\theta_{t,k}-\delta_{ts}\sin\rho_{ts}}{d_{t,k}\cos\theta_{t,k}+\delta_{ts}\cos\rho_{ts}}, \tag{8a}$$

$$\theta_{rs,k} = \arctan\frac{d_{r,k}\sin\theta_{r,k}-\delta_{rs}\sin\rho_{rs}}{d_{r,k}\cos\theta_{r,k}+\delta_{rs}\cos\rho_{rs}}, \tag{8b}$$

$$d_{ts,k} = \sqrt{\delta_{ts}^2+d_{t,k}^2+2\delta_{ts}d_{t,k}\cos\left(\theta_{t,k}+\rho_{ts}\right)}, \tag{8c}$$

$$d_{rs,k} = \sqrt{\delta_{rs}^2+d_{r,k}^2+2\delta_{rs}d_{r,k}\cos\left(\theta_{r,k}+\rho_{rs}\right)}. \tag{8d}$$

The position information $\boldsymbol{p}_{m,k}$ of the vehicle k can be jointly determined by the distances $d_{t,k}$, $d_{r,k}$ and the angles $\theta_{t,k}$, $\theta_{r,k}$. Therefore we define $\boldsymbol{\eta}_k=[d_{t,k},d_{r,k},\theta_{t,k},\theta_{r,k}]^T$ as direct parameter vector for vehicle localization.

B. Optimization problem

The purpose of beamforming is to design a set of directional beams to reduce the power loss of omnidirectional radar and ensure localization performance. In this scenario, the joint active and passive beamforming becomes the problem of minimizing transimt power under the constraints of the vehicle localization accuracy and the RIS's phase parameter matrices $\boldsymbol{\Omega}_t$ and $\boldsymbol{\Omega}_r$, which are adjustable. The performance metric CRB of parameter vectors can be given by the Fishers information matrix (FIM) $\boldsymbol{J}_{p_{m,k}}$ with respect to the location parameter $\boldsymbol{p}_{m,k}$. Specifically, let $\widehat{\boldsymbol{p}}_{m,k}$ indicate the estimated value of the position parameter vector $\boldsymbol{p}_{m,k}$ based on the matched filtered output $\boldsymbol{r}(t)$. The localization accuracy can be given by the mean square error (MSE) of the localization parameter. According to the Cramér-Rao inequality, the MSE of any parameter estimation is not less than the Cramér-Rao lower bound. Therefore, we have

$$E\left[\left(\widehat{\boldsymbol{p}}_{m,k}-\boldsymbol{p}_{m,k}\right)\left(\widehat{\boldsymbol{p}}_{m,k}-\boldsymbol{p}_{m,k}\right)^T\right]\succeq\boldsymbol{J}_{p_{m,k}}^{-1}, \tag{9}$$

and then

$$E\left[\left\|\widehat{\boldsymbol{p}}_{m,k}-\boldsymbol{p}_{m,k}\right\|_2^2\right]\geq tr\left(\boldsymbol{J}_{p_{m,k}}^{-1}\right)\triangleq\boldsymbol{CRB}. \tag{10}$$

Hence, we use CRB as the performance metric to characterize the localization accuracy in the optimization problem. Our aim is to reduce the overall power loss of the system and ensure the localization performance by designing active and passive beamforming. As a result, the beamforming problem with respect to the RIS can be expressed as

$$\begin{aligned}\mathcal{P}_0:\quad &\min_{\boldsymbol{W},\boldsymbol{\Omega}_t,\boldsymbol{\Omega}_r}\ \sum_{k=1}^{K}\left\|\boldsymbol{\omega}_k\right\|_2^2 \\ &s.t.\ \ \boldsymbol{CRB}_k\leq\varepsilon_k, k=1,2,\cdots,K, \\ &\quad\ \ |\vartheta_{t,i}|=1, i=1,2,\cdots,N_{ts}, \\ &\quad\ \ |\vartheta_{r,i}|=1, i=1,2,\cdots,N_{rs}.\end{aligned} \tag{11}$$

where ε denotes the predefined threshold of the localization accuracy, the 2-norms of the radar beamforming vectors for each target represents the radar transmit power [26], [32], and the optimal variables of the problem are $\boldsymbol{W}$, $\boldsymbol{\Omega}_t$ and $\boldsymbol{\Omega}_r$. Specifically, $\boldsymbol{W}$ is the active beamforming variable for transmitter, and $\boldsymbol{\Omega}_t$ and $\boldsymbol{\Omega}_r$ are the passive beamforming variables for RISs.

III. LOCALIZATION PERFORMANCE METRIC

In this section, we analyze the FIM of direct parameter vector $\boldsymbol{\eta}_k$ and relevant Jacobian matrix, and ultimately achieve the CRB of vehicle localization as the performance metric.

For a particular sampling period N_T, the FIM with respect to the direct variable $\boldsymbol{\eta}_k$ can be defined as

$$\boldsymbol{J}_{\eta_k}=E_r\left\{\left[\frac{\partial\ln f\left(\boldsymbol{r}_k|\boldsymbol{\eta}_k\right)}{\partial\boldsymbol{\eta}_k}\right]\left[\frac{\partial\ln f\left(\boldsymbol{r}_k|\boldsymbol{\eta}_k\right)}{\partial\boldsymbol{\eta}_k}\right]^H\right\}, \tag{12}$$

where $f\left(\boldsymbol{r}_k|\boldsymbol{\eta}_k\right)$ is the likelihood function of the formula (7), which can be expressed as

$$f\left(\boldsymbol{r}_k|\boldsymbol{\eta}_k\right)=\exp\left[\frac{2}{\sigma^2}\sum_{N=1}^{N_T}\boldsymbol{r}_k\boldsymbol{H}_k\boldsymbol{\omega}_k-\frac{1}{\sigma^2}\sum_{N=1}^{N_T}\left(\boldsymbol{H}_k\boldsymbol{\omega}_k\right)^2\right]. \tag{13}$$

Then, the FIM $\boldsymbol{J}_{\eta_k}$ with respect to the direct parameter $\boldsymbol{\eta}_k$ can be written as

$$\boldsymbol{J}_{\eta_k}=\begin{bmatrix}\psi_{d_{t,k},d_{t,k}} & \psi_{d_{t,k},d_{r,k}} & \psi_{d_{t,k},\theta_{t,k}} & \psi_{d_{t,k},\theta_{r,k}} \\ \psi_{d_{t,k},d_{r,k}} & \psi_{d_{r,k},d_{r,k}} & \psi_{d_{r,k},\theta_{t,k}} & \psi_{d_{r,k},\theta_{r,k}} \\ \psi_{d_{t,k},\theta_{t,k}} & \psi_{d_{r,k},\theta_{t,k}} & \psi_{\theta_{t,k},\theta_{t,k}} & \psi_{\theta_{t,k},\theta_{t,k}} \\ \psi_{d_{t,k},\theta_{r,k}} & \psi_{d_{r,k},\theta_{r,k}} & \psi_{\theta_{t,k},\theta_{t,k}} & \psi_{\theta_{r,k},\theta_{r,k}}\end{bmatrix}, \tag{14}$$

where the specific elements of the matrix $\boldsymbol{J}_{\eta_k}$ are presented in Appendix A. Furthermore, the FIM $\boldsymbol{J}_{p_{m,k}}$ for the vehicle position parameter $\boldsymbol{p}_{m,k}$ can be represented as

$$\boldsymbol{J}_{p_{m,k}} = \boldsymbol{T}_k \boldsymbol{J}_{\eta_k} \boldsymbol{T}_k^T, \tag{15}$$

where $\boldsymbol{T}_k$ is the Jacobian matrix, which describes the relationship between the position parameter $\boldsymbol{p}_{m,k}$ and the direct parameter $\boldsymbol{\eta}_k$. The specific geometric relationships of $\boldsymbol{p}_{m,k}$ and $\boldsymbol{\eta}_k$ are as follows

$$d_{t,k} = \|\boldsymbol{p}_t - \boldsymbol{p}_{m,k}\|_2, \tag{16a}$$
$$d_{r,k} = \|\boldsymbol{p}_r - \boldsymbol{p}_{m,k}\|_2, \tag{16b}$$
$$\theta_{t,k} = \arcsin\left[(p_{tx} - p_{mx,k})/\|\boldsymbol{p}_t - \boldsymbol{p}_{m,k}\|_2\right], \tag{16c}$$
$$\theta_{r,k} = \arcsin\left[(p_{rx} - p_{mx,k})/\|\boldsymbol{p}_r - \boldsymbol{p}_{m,k}\|_2\right]. \tag{16d}$$

The Jacobian matrix $\boldsymbol{T}_k$ can be written as

$$\boldsymbol{T}_k = \begin{bmatrix} \frac{\partial d_{t,k}}{\partial p_{mx,k}} & \frac{\partial d_{r,k}}{\partial p_{mx,k}} & \frac{\partial \theta_{t,k}}{\partial p_{mx,k}} & \frac{\partial \theta_{r,k}}{\partial p_{mx,k}} \\ \\ \frac{\partial d_{t,k}}{\partial p_{my,k}} & \frac{\partial d_{r,k}}{\partial p_{my,k}} & \frac{\partial \theta_{t,k}}{\partial p_{my,k}} & \frac{\partial \theta_{r,k}}{\partial p_{my,k}} \end{bmatrix}, \tag{17}$$

and the specific matrix elements of the matrix $\boldsymbol{T}_k$ can be given by

$$\frac{\partial d_{t,k}}{\partial p_{mx,k}} = \frac{p_{mx,k} - p_{tx}}{\|\boldsymbol{p}_t - \boldsymbol{p}_{m,k}\|_2}, \tag{18a}$$
$$\frac{\partial d_{t,k}}{\partial p_{my,k}} = \frac{p_{my,k} - p_{ty}}{\|\boldsymbol{p}_t - \boldsymbol{p}_{m,k}\|_2}, \tag{18b}$$
$$\frac{\partial d_{r,k}}{\partial p_{mx,k}} = \frac{p_{mx,k} - p_{rx}}{\|\boldsymbol{p}_r - \boldsymbol{p}_{m,k}\|_2}, \tag{18c}$$
$$\frac{\partial d_{r,k}}{\partial p_{my,k}} = \frac{p_{my,k} - p_{ry}}{\|\boldsymbol{p}_r - \boldsymbol{p}_{m,k}\|_2}, \tag{18d}$$
$$\frac{\partial \theta_{t,k}}{\partial p_{mx,k}} = \frac{p_{my,k} - p_{ty}}{\|\boldsymbol{p}_t - \boldsymbol{p}_{m,k}\|_2^2}, \tag{18e}$$
$$\frac{\partial \theta_{t,k}}{\partial p_{my,k}} = -\frac{p_{mx,k} - p_{tx}}{\|\boldsymbol{p}_t - \boldsymbol{p}_{m,k}\|_2^2}, \tag{18f}$$
$$\frac{\partial \theta_{r,k}}{\partial p_{mx,k}} = \frac{p_{my,k} - p_{ry}}{\|\boldsymbol{p}_r - \boldsymbol{p}_{m,k}\|_2^2}, \tag{18g}$$
$$\frac{\partial \theta_{r,k}}{\partial p_{my,k}} = -\frac{p_{mx,k} - p_{tx}}{\|\boldsymbol{p}_r - \boldsymbol{p}_{m,k}\|_2^2}, \tag{18h}$$

Therefore, the localization performance metric CRB can be obtained by the inverse of the FIM $\boldsymbol{J}_{p_{m,k}}$, i.e,

$$\boldsymbol{CRB} = tr\left(\boldsymbol{J}_{p_{m,k}}^{-1}\right). \tag{19}$$

IV. Single Vehicle Beamforming Optimization

In this section, we investigate the beamforming optimization problem in the single vehicle setup, that is, K=1. We propose a SVBO method and obtain joint active and passive beamforming optimal result in the case. Since the number of vehicles is one, the problem $\mathcal{P}_0$ can be reduced to

$$\begin{aligned} \mathcal{P}_1: \quad & \min_{\boldsymbol{\omega}_1, \boldsymbol{\Omega}_t, \boldsymbol{\Omega}_r} \ \|\boldsymbol{\omega}_1\|_2^2 \\ & s.t. \ tr\left(\boldsymbol{J}_{p_{m,1}}^{-1}\right) \le \varepsilon_1, \\ & |\vartheta_{t,i}| = 1, i = 1, 2, \cdots, N_{ts}, \\ & |\vartheta_{r,i}| = 1, i = 1, 2, \cdots, N_{rs}, \end{aligned} \tag{20}$$

where $\boldsymbol{\omega}_1 \in \mathbb{C}^{N_t \times 1}$ is the beamforming vector of a single vehicle. The problem $\mathcal{P}_1$ is a non-convex problem under the parameters $\boldsymbol{\omega}_1, \boldsymbol{\Omega}_t, \boldsymbol{\Omega}_r$. It is worth pointing out that the passive beamforming of the two RISs in the single-vehicle scenario no longer requires the overall performance considerations of multiple vehicles, but only needs to point to a specific vehicle direction. Therefore, in the next two subsections, we can obtain the optimal phase of passive beamforming by using the beam pattern, and then derive the optimal solution of active beamforming on this basis.

A. Passive Beamforming Design

Proposition 1. *When the two RISs' phases meet*

$$\phi_{t,i} = \frac{2\pi(i-1) f_c d}{c} \left(\sin\theta_{ts,1} + \sin\delta_{ts}\right), i = 1, 2, \cdots, N_{ts}, \tag{21a}$$

$$\phi_{r,i} = \frac{2\pi(i-1) f_c d}{c} \left(\sin\theta_{rs,1} + \sin\delta_{rs}\right), i = 1, 2, \cdots, N_{rs}, \tag{21b}$$

respectively, we can obtain the optimal solution of the passive beamforming variables $\boldsymbol{\Omega}_t$ and $\boldsymbol{\Omega}_r$ in problem $\mathcal{P}_1$.

Proof. The gain Υ_t from the transmitter to the vehicle through RIS, and the gain Υ_r from the vehicle to the receiver through RIS can be separately defined as

$$\Upsilon_t = \frac{1}{N_{ts}} \sum_{i=0}^{N_{ts}-1} e^{j\left(\phi_{t,i} - \frac{2\pi(i-1) f_c d \sin\theta_{ts,1}}{c} - \frac{2\pi(i-1) f_c d \sin\delta_{ts}}{c}\right)}, \tag{22a}$$

$$\Upsilon_t = \frac{1}{N_{rs}} \sum_{i=0}^{N_{rs}-1} e^{j\left(\phi_{r,i} - \frac{2\pi(i-1) f_c d \sin\theta_{rs,1}}{c} - \frac{2\pi(i-1) f_c d \sin\delta_{rs}}{c}\right)}. \tag{22b}$$

We define $\varphi_{t,i} = \frac{2\pi(i-1) f_c d \sin\theta_{ts,1}}{c} + \frac{2\pi(i-1) f_c d \sin\delta_{ts}}{c}$ and $\varphi_{r,i} = \frac{2\pi(i-1) f_c d \sin\theta_{rs,1}}{c} + \frac{2\pi(i-1) f_c d \sin\delta_{rs}}{c}$, and use the characteristics of the proportional sequence to obtain the gain results as follows

$$\frac{1}{N_{ts}} \sum_{i=0}^{N_{ts}-1} e^{j\left(\phi_{t,i} - \varphi_{t,i}\right)} = \begin{cases} \left| \frac{\cos\left(N_{ts}\left(\phi_{t,i} - \varphi_{t,i}\right)/2\right)}{N_{ts}\cos\left(\left(\phi_{t,i} - \varphi_{t,i}\right)/2\right)} \right|, & if \ \ \phi_{t,i} - \varphi_{t,i} \neq 0, \\ 1, & if \ \ \phi_{t,i} - \varphi_{t,i} = 0, \end{cases} \tag{23a}$$

$$\frac{1}{N_{rs}} \sum_{i=0}^{N_{rs}-1} e^{j\left(\phi_{r,i} - \varphi_{r,i}\right)} = \begin{cases} \left| \frac{\cos\left(N_{rs}\left(\phi_{r,i} - \varphi_{r,i}\right)/2\right)}{N_{rs}\cos\left(\left(\phi_{r,i} - \varphi_{r,i}\right)/2\right)} \right|, & if \ \ \phi_{r,i} - \varphi_{r,i} \neq 0, \\ 1, & if \ \ \phi_{r,i} - \varphi_{r,i} = 0. \end{cases} \tag{23b}$$

Therefore, when $\phi_{t,i} = \varphi_{t,i}, i = 1, 2, \cdots, N_{ts}$ and $\phi_{r,i} = \varphi_{r,i}, i = 1, 2, \cdots, N_{rs}$, the signal strength for the vehicle reaches the maximum, and the passive beamforming design

of the two RISs is fully adapted to the unique vehicle. Then, we obtain the optimal solution for passive beamforming under variables $\mathbf{\Omega}_t$ and $\mathbf{\Omega}_r$. This complete the proof of *Proposition 1*. □

***Remark* 1.** Proposition 1 *is the optimal result of passive beamforming in the single vehicle situation. It is worth emphasizing that the solution of the passive beamforming problem in the single vehicle scenario provides us with the best performance metric in the RIS-assisted vehicle localization scenario. This result effectively solves the coupling problem of the RIS phase variables $\mathbf{\Omega}_t$ and $\mathbf{\Omega}_r$ in the original problem. Therefore, in the next subsection, our performance metric CRB will be simplified by removing the coupling variables $\mathbf{\Omega}_t$ and $\mathbf{\Omega}_r$ to effectively solve the active beamforming problem.*

B. Active Beamforming Optimization

By introducing *Proposition 1* into the problem $\mathcal{P}_1$, the active beamforming optimization problem can be simplified as

$$\begin{aligned}\mathcal{P}_2: \quad & \min_{\boldsymbol{\omega}_1} \ \|\boldsymbol{\omega}_1\|_2^2 \\ & s.t. \ tr\left(\bar{\boldsymbol{J}}_{p_{m,1}}^{-1}\right) \le \varepsilon_1,\end{aligned} \tag{24}$$

where $\bar{\boldsymbol{J}}_{p_{m,1}}^{-1}$ is the CRB without the RISs' phase parameter. In the single vehicle scenario, our performance metric CRB is expressed as [47], [48]

$$tr\left(\bar{\boldsymbol{J}}_{p_{m,1}}^{-1}\right) = \frac{\sigma^2 tr\left(\boldsymbol{H}_1^H \boldsymbol{H}_1 \boldsymbol{\omega}_1 \boldsymbol{\omega}_1^H\right)}{2N_T\left(tr\left(\dot{\boldsymbol{H}}_1^H \dot{\boldsymbol{H}}_1 \boldsymbol{\omega}_1 \boldsymbol{\omega}_1^H\right) tr\left(\boldsymbol{H}_1^H \boldsymbol{H}_1 \boldsymbol{\omega}_1 \boldsymbol{\omega}_1^H\right) - \left|tr\left(\dot{\boldsymbol{H}}_1^H \boldsymbol{H}_1 \boldsymbol{\omega}_1 \boldsymbol{\omega}_1^H\right)\right|^2\right)}, \tag{25}$$

where $\dot{\boldsymbol{H}}_1 = \frac{\partial \boldsymbol{H}_1}{\partial \boldsymbol{p}_{m,1}}$. Here, we define

$$\boldsymbol{h}_{t,1} = \boldsymbol{v}_{t,1}\gamma_{t,1} + \boldsymbol{G}_t \mathbf{\Omega}_t \boldsymbol{v}_{ts,1}\gamma_{ts,1}, \tag{26a}$$

$$\boldsymbol{h}_{r,1} = \boldsymbol{v}_{r,1}\gamma_{r,1} + \boldsymbol{G}_r \mathbf{\Omega}_r \boldsymbol{v}_{rs,1}\gamma_{rs,1}, \tag{26b}$$

$$\dot{\boldsymbol{h}}_{t,1} = \frac{\partial \boldsymbol{h}_{t,1}}{\partial \boldsymbol{p}_{m,1}}, \tag{26c}$$

$$\dot{\boldsymbol{h}}_{r,1} = \frac{\partial \boldsymbol{h}_{r,1}}{\partial \boldsymbol{p}_{m,1}}. \tag{26d}$$

Then, the elements in (25) can be expressed in (27). Subsituting (27) into (25), $tr\left(\bar{\boldsymbol{J}}_{p_{m,1}}^{-1}\right)$ can be processed as

$$tr\left(\bar{\boldsymbol{J}}_{p_{m,1}}^{-1}\right) = \frac{\sigma^2}{2N_T\left\|\dot{\boldsymbol{h}}_{r,1}\right\|^2\left|\boldsymbol{h}_{t,1}^H\boldsymbol{\omega}_1\right|^2}. \tag{28}$$

Then, the problem $\mathcal{P}_2$ can be recast as

$$\begin{aligned}& \min_{\boldsymbol{\omega}_1} \ \|\boldsymbol{\omega}_1\|_2^2 \\ & s.t. \ \left|\boldsymbol{h}_{t,1}^H\boldsymbol{\omega}_1\right|^2 \ge \frac{\sigma^2}{2N_T\left\|\dot{\boldsymbol{h}}_{r,1}\right\|^2\varepsilon_1}.\end{aligned} \tag{29}$$

As a result, the problem $\mathcal{P}_2$ is simplified as a non-convex quadratically constrained quadratic program (QCQP) problem. We define $\boldsymbol{W}_1 = \boldsymbol{\omega}_1\boldsymbol{\omega}_1^H$ and $\boldsymbol{H}_{t,1} = \boldsymbol{h}_{t,1}\boldsymbol{h}_{t,1}^H$, the problem $\mathcal{P}_2$ can be further written as

$$\begin{aligned}& \min_{\boldsymbol{W}_1 \succeq 0} \ tr\left(\boldsymbol{W}_1\right) \\ & s.t. \ tr\left(\boldsymbol{H}_{t,1}\boldsymbol{W}_1\right) \ge \frac{\sigma^2}{2N_T\left\|\dot{\boldsymbol{h}}_{r,1}\right\|^2\varepsilon_1}, \\ & \quad rank\left(\boldsymbol{W}_1\right) = 1.\end{aligned} \tag{30}$$

At present, the problem $\mathcal{P}_2$ is still a non-convex problem due to the constraint $rank\left(\boldsymbol{W}_1\right) = 1$. Subsequently, by using the convex release technology, the problem $\mathcal{P}_2$ can be released as

$$\begin{aligned}\mathcal{P}_3: \quad & \min_{\boldsymbol{W}_1 \succeq 0} \ tr\left(\boldsymbol{W}_1\right) \\ & s.t. \ tr\left(\boldsymbol{H}_{t,1}\boldsymbol{W}_1\right) \ge \frac{\sigma^2}{2N_T\left\|\dot{\boldsymbol{h}}_{r,1}\right\|^2\varepsilon_1},\end{aligned} \tag{31}$$

Here, the problem $\mathcal{P}_3$ is a standard semidefinite programming (SDP) problem, which can be solved by convex optimization toolbox. According to the perspective of convex release, the optimal solution of problem $\mathcal{P}_3$ is the suboptimal solution of the original problem $\mathcal{P}_2$. Thus, we should pay attention to whether the optimal solution of the problem $\mathcal{P}_3$ satisfies $rank\left(\boldsymbol{W}_1\right) = 1$ to determine the relationship between the problem $\mathcal{P}_2$ and problem $\mathcal{P}_3$.

***Proposition* 2.** *The optimal solution $\boldsymbol{W}_1$ for problem $\mathcal{P}_3$ satisfies $rank\left(\boldsymbol{W}_1\right) = 1$.*

Proof. See Appendix B. □

According to *Proposition 2*, we know the optimal solution of the problem $\mathcal{P}_3$ satisfies $rank\left(\boldsymbol{W}_1\right) = 1$, i.e., the problem $\mathcal{P}_2$ and problem $\mathcal{P}_3$ are equivalent, and their optimal solutions correspond to each other. The optimal solution $\boldsymbol{W}_1^*$ of problem $\mathcal{P}_3$ can be achieved by SDP solver. By using the special value decomposition, $\boldsymbol{W}_1^*$ can be expressed as

$$\boldsymbol{W}_1^* = \alpha^*\boldsymbol{\omega}^*\boldsymbol{\omega}^{*^H}, \tag{32}$$

and the optimal solution of problem $\mathcal{P}_2$ can be written as

---

$$tr\left(\boldsymbol{H}_1^H\boldsymbol{H}_1\boldsymbol{\omega}_1\boldsymbol{\omega}_1^H\right) = tr\left(\boldsymbol{h}_{r,1}\boldsymbol{h}_{t,1}^H\boldsymbol{\omega}_1\boldsymbol{\omega}_1^H\boldsymbol{h}_{t,1}\boldsymbol{h}_{r,1}^H\right) = \|\boldsymbol{h}_{r,1}\|^2\left|\boldsymbol{h}_{t,1}^H\boldsymbol{\omega}_1\right|^2, \tag{27a}$$

$$tr\left(\dot{\boldsymbol{H}}_1^H\boldsymbol{H}_1\boldsymbol{\omega}_1\boldsymbol{\omega}_1^H\right) = tr\left(\boldsymbol{h}_{r,1}\boldsymbol{h}_{t,1}^H\boldsymbol{\omega}_1\boldsymbol{\omega}_1^H\left(\boldsymbol{h}_{t,1}\dot{\boldsymbol{h}}_{r,1}^H + \dot{\boldsymbol{h}}_{t,1}\boldsymbol{h}_{r,1}^H\right)\right) = \|\boldsymbol{h}_{r,1}\|^2\boldsymbol{h}_{t,1}^H\boldsymbol{\omega}_1\boldsymbol{\omega}_1^H\dot{\boldsymbol{h}}_{t,1}, \tag{27b}$$

$$tr\left(\dot{\boldsymbol{H}}_1^H\dot{\boldsymbol{H}}_1\boldsymbol{\omega}_1\boldsymbol{\omega}_1^H\right) = tr\left(\left(\dot{\boldsymbol{h}}_{r,1}\boldsymbol{h}_{t,1}^H + \boldsymbol{h}_{r,1}\dot{\boldsymbol{h}}_{t,1}^H\right)\boldsymbol{\omega}_1\boldsymbol{\omega}_1^H\left(\boldsymbol{h}_{t,1}\dot{\boldsymbol{h}}_{r,1}^H + \dot{\boldsymbol{h}}_{t,1}\boldsymbol{h}_{r,1}^H\right)\right) = \left\|\dot{\boldsymbol{h}}_{r,1}\right\|^2\left|\boldsymbol{h}_{t,1}^H\boldsymbol{\omega}_1\right|^2 + \|\boldsymbol{h}_{r,1}\|^2\left|\dot{\boldsymbol{h}}_{t,1}^H\boldsymbol{\omega}_1\right|^2. \tag{27c}$$

$$\boldsymbol{\omega}_1^* = \sqrt{\alpha^*}\boldsymbol{\omega}^*. \tag{33}$$

Here, we obtain the optimal solution for active beamforming in single vehicle scenario. Furthermore, we emphasize that the computation complexity of this optimization consists of passive beamforming and active beamforming. Since the results of passive beamforming are analytical, the complexity of this method mainly depends on the SDP program of the formula (31). The number of the variables in the problem $\mathcal{P}_3$ is N_t^2, and the complexity is $\mathcal{O}\left(\left(N_t^2+1\right)^{4.5}\right)$. Although this optimization method has low complexity, it can not be directly extended to the multiple vehicles situation. The reason is that we can not intuitively obtain the optimal RIS phase through the beam pointing expression relationship in the multiple vehicles situation. Therefore, in the next section, we propose a new method to solve the joint active and passive beamforming problem in the multiple vehicles scenario.

V. Multiple Vehicles Beamforming Algorithm

In this section, we investigate the beamforming problem in multiple vehicles scenario. The method in Section IV can not be directly extended to this section due to the model complexity caused by multiple vehicles. For the multiple vehicles scenario, we transform the complex original problem into several subproblems, and solve each subproblem through equivalent transformation and convex release. The final optimization solution is obtained when the alternating iteration converges.

A. Alternating Optimization

The beamforming problem in multiple vehicles scenario can be presented by the problem $\mathcal{P}_0$ with rewriting the CRB constraint here

$$\begin{aligned}\mathcal{P}_0: \quad & \min_{\boldsymbol{W},\boldsymbol{\Omega}_t,\boldsymbol{\Omega}_r} \sum_{k=1}^{K}\|\boldsymbol{\omega}_k\|_2^2 \\ & s.t.\ \ \boldsymbol{C}_1: tr\left(\boldsymbol{J}_{p_{m,k}}^{-1}\right) \le \varepsilon_k, k=1,2,\cdots,K, \\ & \qquad \boldsymbol{C}_2: |\vartheta_{t,i}| = 1, i=1,2,\cdots,N_{ts}, \\ & \qquad \boldsymbol{C}_3: |\vartheta_{r,i}| = 1, i=1,2,\cdots,N_{rs}.\end{aligned} \tag{34}$$

Obviously, the problem $\mathcal{P}_0$ is the non-convex problem with respect to the optimization variables $\boldsymbol{W}$, $\boldsymbol{\Omega}_t$ and $\boldsymbol{\Omega}_r$. In particular, the coupled relation between $\boldsymbol{\omega}_k$, $\boldsymbol{\Omega}_t$ and $\boldsymbol{\Omega}_r$ is so complicated that it is hard to obtain a convex form. We underline that although the phase constraints of the two RISs are separable in constraint $\boldsymbol{C}_2$ and $\boldsymbol{C}_3$, they are deeply coupled in constraint $\boldsymbol{C}_1$. Therefore, we use alternate optimization to rewrite the original problem $\mathcal{P}_0$ into the following two subproblems $\mathcal{P}_4$ and $\mathcal{P}_5$

$$\begin{aligned}\mathcal{P}_4: \quad & \min_{\boldsymbol{W},\boldsymbol{\Omega}_t} \sum_{k=1}^{K}\|\boldsymbol{\omega}_k\|_2^2 \\ & s.t.\ \ tr\left(\boldsymbol{J}_{p_{m,k}}^{-1}\right) \le \varepsilon_k, k=1,2,\cdots,K, \\ & \qquad |\vartheta_{t,i}| = 1, i=1,2,\cdots,N_{ts}.\end{aligned} \tag{35}$$

$$\begin{aligned}\mathcal{P}_5: \quad & \min_{\boldsymbol{W},\boldsymbol{\Omega}_r} \sum_{k=1}^{K}\|\boldsymbol{\omega}_k\|_2^2 \\ & s.t.\ \ tr\left(\boldsymbol{J}_{p_{m,k}}^{-1}\right) \le \varepsilon_k, k=1,2,\cdots,K, \\ & \qquad |\vartheta_{r,i}| = 1, i=1,2,\cdots,N_{rs}.\end{aligned} \tag{36}$$

Note that $\mathcal{P}_4$ works when the phase $\boldsymbol{\Omega}_r$ is fixed in $\mathcal{P}_0$ and $\mathcal{P}_5$ is valid when $\boldsymbol{\Omega}_t$ is given. The mathematical expressions of the problem $\mathcal{P}_4$ and the problem $\mathcal{P}_5$ are symmetric. Consequently, the two optimization problems can be solved separately with the same optimization method in their separate parts.

B. Partial Variable Optimization

Taking the problem $\mathcal{P}_4$ as an example, we emphasize that optimization variables $\boldsymbol{\omega}_k$ and $\boldsymbol{\Omega}_t$ are still coupled, and it is difficult to give a closed expression of the CRB. According to [49], we always have

$$\inf_{x,y} f(x,y) = \inf_{x} \tilde{f}(x), \tag{37}$$

where $\tilde{f}(x) = \inf_{y} f(x,y)$. In other words, we can always minimize a function by first minimizing over some of the variables, and then minimizing over the remaining ones. Here, we first optimize the passive beamforming variable $\boldsymbol{\Omega}_t$. In order to avoid complex matrix inversion, we introduce an auxiliary matrix $\boldsymbol{A}$, and use Schur complement method to handle the matrix inversion into a positive semi-definite constraint [50]. In addition, we notice that the phase constraint of RIS is still non-convex. We rewrite the phase expression as $\boldsymbol{\phi}_t = \left[e^{j\phi_1}, e^{j\phi_2}, \cdots, e^{j\phi_{N_{ts}}}\right]^T$, and define $\boldsymbol{\Phi}_t = \boldsymbol{\phi}_t\boldsymbol{\phi}_t^H$, which satisfies $\boldsymbol{\Phi}_t \succeq 0$ and $rank\left(\boldsymbol{\Phi}_t\right) = 1$. Since the rank-one constraint is non-convex, we need to relax the original phase constraint and the problem $\mathcal{P}_4$ can be released as

$$\begin{aligned}\mathcal{P}_6: \quad & \min_{\boldsymbol{\Omega}_t} \sum_{k=1}^{K}\|\boldsymbol{\omega}_k\|_2^2 \\ & \begin{bmatrix} \boldsymbol{A}_k & \boldsymbol{I}_2 \\ \boldsymbol{I}_2 & \boldsymbol{J}_{p_{m,k}} \end{bmatrix} \succeq 0, k=1,2,\cdots,K, \\ & tr\left(\boldsymbol{A}_k\right) \le \varepsilon_k, k=1,2,\cdots,K, \\ & \boldsymbol{J}_{p_{m,k}} \succeq 0, k=1,2,\cdots,K, \\ & \boldsymbol{\Phi}_{t,i,i} = 1, i=1,2,\cdots,N_{ts}, \\ & \boldsymbol{\Phi}_t \succeq 0,\end{aligned} \tag{38}$$

where $\boldsymbol{I}_2$ denotes an identity matrix of order 2. It is worth emphasizing that the objective function in the problem $\mathcal{P}_6$ does not contain optimization variable $\boldsymbol{\Omega}_t$. Thus, it is a feasible SDP optimization problem, and can be effectively solved by using some toolboxes such as CVX [51]. Additionally, as a release of the original phase constraint, solving the problem $\mathcal{P}_6$ can just obtain the suboptimal solution of the original phase problem. [52] shows that the SDR method can guarantee the $\pi/4$ approximation of the optimal value of the program under the condition of sufficient randomization which indicates that our SDP problem $\mathcal{P}_6$ is valid in this passive beamforming

problem. With the solution of the problem $\mathcal{P}_6$, we can realize the optimal phase shift of the RIS and obtain the corresponding FIM $\tilde{\boldsymbol{J}}_{p_{m,k}}$ without the phase matrix $\boldsymbol{\Omega}_t$. After optimizing variable $\boldsymbol{\Omega}_t$, the problem $\mathcal{P}_4$ can be written as $\mathcal{P}_7$

$$\begin{aligned}\mathcal{P}_7: \quad & \min_{\boldsymbol{W}} \ \sum_{k=1}^{K} \|\boldsymbol{\omega}_k\|_2^2 \\ & s.t. \ tr\left(\tilde{\boldsymbol{J}}_{p_{m,k}}^{-1}\right) \leq \varepsilon_k, k=1,2,\cdots,K.\end{aligned} \tag{39}$$

Note that the optimization variable $\boldsymbol{\omega}_k$ in the FIM information matrix element in Appendix A is multiplied at the beginning and end of the matrix $\boldsymbol{J}_{\eta_k}$. Therefore, we can take out the variable $\boldsymbol{\omega}_k$, select any feasible solution $\boldsymbol{\Omega}_t$ in the phase feasible set, and define the remaining part as matrices $\boldsymbol{Q}_{i,k}, i=1,2,3$. In this case, the FIM $\tilde{\boldsymbol{J}}_{p_{m,k}}$ can be expressed as

$$\tilde{\boldsymbol{J}}_{p_{m,k}} = \begin{bmatrix} \boldsymbol{\omega}_k^H \boldsymbol{Q}_{1,k} \boldsymbol{\omega}_k & \boldsymbol{\omega}_k^H \boldsymbol{Q}_{2,k} \boldsymbol{\omega}_k \\ \boldsymbol{\omega}_k^H \boldsymbol{Q}_{2,k} \boldsymbol{\omega}_k & \boldsymbol{\omega}_k^H \boldsymbol{Q}_{3,k} \boldsymbol{\omega}_k \end{bmatrix}. \tag{40}$$

Since $\tilde{\boldsymbol{J}}_{p_{m,k}} \in \mathbb{C}^{2\times 2}$, we can naturally obtain its specific analytical expression after some manipulations. Then, the optimization problem $\mathcal{P}_7$ can be rewritten as

$$\begin{aligned}\mathcal{P}_7': \min_{\boldsymbol{W}} \ & \sum_{k=1}^{K} \|\boldsymbol{\omega}_k\|_2^2 \\ s.t. \ & \frac{\boldsymbol{\omega}_k^H \boldsymbol{Q}_{1,k} \boldsymbol{\omega}_k + \boldsymbol{\omega}_k^H \boldsymbol{Q}_{3,k} \boldsymbol{\omega}_k}{\boldsymbol{\omega}_k^H \boldsymbol{Q}_{1,k} \boldsymbol{\omega}_k \boldsymbol{\omega}_k^H \boldsymbol{Q}_{3,k} \boldsymbol{\omega}_k - \boldsymbol{\omega}_k^H \boldsymbol{Q}_{2,k} \boldsymbol{\omega}_k \boldsymbol{\omega}_k^H \boldsymbol{Q}_{2,k} \boldsymbol{\omega}_k} \leq \varepsilon_k, \\ & k=1,2,\cdots,K.\end{aligned} \tag{41}$$

It should be pointed out that the form of the variable $\boldsymbol{\omega}_k$ is $\boldsymbol{\omega}_k = [\omega_{1,k}, \omega_{2,k}, \cdots, \omega_{N_T,k}]^H$. Define $\boldsymbol{U}_k = \boldsymbol{\omega}_k \boldsymbol{\omega}_k^H$, and we can obtain $tr(\boldsymbol{U}_k) = \boldsymbol{\omega}_k^H \boldsymbol{\omega}_k$. Subsequently, the problem $\mathcal{P}_7'$ can be given by

$$\begin{aligned}\mathcal{P}_7'': \min_{\boldsymbol{U}_k} \ & \sum_{k=1}^{K} tr(\boldsymbol{U}_k) \\ s.t. \ & \frac{tr(\boldsymbol{Q}_{1,k}\boldsymbol{U}_k) + tr(\boldsymbol{Q}_{3,k}\boldsymbol{U}_k)}{tr(\boldsymbol{Q}_{1,k}\boldsymbol{U}_k\boldsymbol{Q}_{3,k}\boldsymbol{U}_k) - tr(\boldsymbol{Q}_{2,k}\boldsymbol{U}_k\boldsymbol{Q}_{2,k}\boldsymbol{U}_k)} \leq \varepsilon_k, \\ & k=1,2,\cdots,K.\end{aligned} \tag{42}$$

It is not difficult to find that the relationship between the main diagonal element of the matrix $\boldsymbol{U}_k$ and the original variable $\boldsymbol{\omega}_k$ is as follows

$$\boldsymbol{U}_{k,i,i} = u_{i,k} = \omega_{i,k}^2. \tag{43}$$

Then, the optimization problem $\mathcal{P}_7''$ can be further written as

Algorithm 1: Multiple Vehicle Beanmforming Algorithm

1: Provide iteration stop threshold ξ;
2: Initialize RIS phases $\boldsymbol{\Omega}_t$ and $\boldsymbol{\Omega}_r$;
3: **repeat**
4: Fix $\boldsymbol{\Omega}_r$;
5: Solve the convex feasibility problem (38);
6: Obtain the beamforming result $\boldsymbol{W}_t$ from (45);
7: Update $\boldsymbol{\Omega}_t$ with the results of step 5;
8: Fix $\boldsymbol{\Omega}_r$;
9: Solve the convex feasibility problem similar to (38);
10: Obtain the beamforming result $\boldsymbol{W}_r$ similar to (45);
11: Update $\boldsymbol{\Omega}_t$ with the results of step 9;
12:**until** $\|\boldsymbol{W}_t - \boldsymbol{W}_r\|_F \leq \xi$
13:Output $\boldsymbol{W}^* = \boldsymbol{W}_t$ or $\boldsymbol{W}^* = \boldsymbol{W}_r$.

$$\begin{aligned}\mathcal{P}_7''': \min_{\boldsymbol{U}_k} \ & \sum_{k=1}^{K} \sum_{i=1}^{N_T} u_{i,k} \\ s.t. \ & \frac{\sum\limits_{i,j=1}^{N_T} (\boldsymbol{Q}_{1,k} + \boldsymbol{Q}_{3,k})_{ij,k} u_{i,k}}{\sum\limits_{i,j=1}^{N_T} (\boldsymbol{Q}_{1,k}\boldsymbol{Q}_{3,k} - \boldsymbol{Q}_{2,k}\boldsymbol{Q}_{2,k})_{ij,k} u_{i,k}^2} \leq \varepsilon_k, \\ & k=1,2,\cdots,K.\end{aligned} \tag{44}$$

By introducing variables $\boldsymbol{Z}_k$ and t, and using the convexity preserving property of perspective function, the problem $\mathcal{P}_7'''$ can be equivalently transformed into the following optimization problem

$$\begin{aligned}\mathcal{P}_8: \quad & \min_{\boldsymbol{Z}_k, t} \ \sum_{k=1}^{K} \sum_{i=1}^{N_T} z_{i,k} \\ & s.t. \ \sum_{i,j=1}^{N_T} (\boldsymbol{Q}_{1,k} + \boldsymbol{Q}_{3,k})_{ij,k} z_{i,k} \leq -1, \\ & \sum_{i,j=1}^{N_T} (\boldsymbol{Q}_{1,k}\boldsymbol{Q}_{3,k} - \boldsymbol{Q}_{2,k}\boldsymbol{Q}_{2,k})_{ij,k} \frac{z_{i,k}^2}{t} \leq \varepsilon_k, \\ & k=1,2,\cdots,K.\end{aligned} \tag{45}$$

The above optimization problem is a feasible GP, and can be effectively solved by using convex optimization toolboxes.

C. Overall Algorithm

Based on the results in previous two subsections, the passive and active beamforming problems in the problem $\mathcal{P}_4$ are solved through the problem $\mathcal{P}_6$ and problem $\mathcal{P}_8$, respectively, and this algorithm is also applicable to the problem $\mathcal{P}_5$. The complete MVBA is shown in $\boldsymbol{Algorithm\ 1}$.

***Remark* 2.** *Since the optimization variables $\boldsymbol{\omega}_k$, $\boldsymbol{\Omega}_t$ and $\boldsymbol{\Omega}_r$ in the problem $\mathcal{P}_0$ are deeply coupled in the constraint $\boldsymbol{C}_1$, it is difficult to directly solve the beamforming problem under vehicle localization system. We can see that although the variables $\boldsymbol{\Omega}_t$ and $\boldsymbol{\Omega}_r$ are coupled in the optimization problem, they*

do not affect each other in the other constraints. Therefore, the problem $\mathcal{P}_0$ can be decomposed into the subproblems $\mathcal{P}_4$ and $\mathcal{P}_5$ for alternative solution. In each subproblem, the phase optimization variable $\mathbf{\Omega}_t$ (or $\mathbf{\Omega}_r$) and the beamforming optimization variable $\boldsymbol{\omega}_k$ are coupled by multiplication. The passive beamforming optimization first considers only the optimization variable $\mathbf{\Omega}_t$ (or $\mathbf{\Omega}_r$), thus obtaining the feasible set of RIS's phase. Using the optimized set of phase feasible solutions, the active beamforming problem is simplified and eventually transformed into GP form to solve. The overall problem is solved alternately until the result converges.

Convergence: We discuss the convergence of $\boldsymbol{Algorithm\ 1}$ as follows.

Since the optimal solution of problems $\mathcal{P}_6$ and $\mathcal{P}_8$ are obtained, we have

$$\begin{aligned}\sum_{k=1}^{K}\|\boldsymbol{\omega}_k\|_2^2\left(\boldsymbol{W}^i,\mathbf{\Omega}_t^i,\mathbf{\Omega}_r^i\right)&\overset{(a)}{\geq}\sum_{k=1}^{K}\|\boldsymbol{\omega}_k\|_2^2\left(\boldsymbol{W}^i,\mathbf{\Omega}_t^{i+1},\mathbf{\Omega}_r^i\right)\\&\overset{(b)}{\geq}\sum_{k=1}^{K}\|\boldsymbol{\omega}_k\|_2^2\left(\boldsymbol{W}^{i+0.5},\mathbf{\Omega}_t^{i+1},\mathbf{\Omega}_r^i\right)\\&\overset{(c)}{\geq}\sum_{k=1}^{K}\|\boldsymbol{\omega}_k\|_2^2\left(\boldsymbol{W}^{i+0.5},\mathbf{\Omega}_t^{i+1},\mathbf{\Omega}_r^{i+1}\right)\\&\overset{(b)}{\geq}\sum_{k=1}^{K}\|\boldsymbol{\omega}_k\|_2^2\left(\boldsymbol{W}^{i+1},\mathbf{\Omega}_t^{i+1},\mathbf{\Omega}_r^{i+1}\right).\end{aligned}\tag{46}$$

where (a) holds because the problem $\mathcal{P}_6$ is a convex feasibility problem. For any feasible solution $\mathbf{\Omega}_t^{i+1}$ to problem $\mathcal{P}_6$, it satisfies $\sum_{k=1}^{K}\|\boldsymbol{\omega}_k\|_2^2\left(\boldsymbol{W}^i,\mathbf{\Omega}_t^i,\mathbf{\Omega}_r^i\right)\geq\sum_{k=1}^{K}\|\boldsymbol{\omega}_k\|_2^2\left(\boldsymbol{W}^i,\mathbf{\Omega}_t^{i+1},\mathbf{\Omega}_r^i\right)$, where $\mathbf{\Omega}_t^i$ is the result of the previous iteration. Similar conclusions also apply to (c). As the problem $\mathcal{P}_8$ is a GP form convex optimization problem, in each round of alternating iterations, the minimum value of the objective function corresponds to the optimal solution of problem the problem $\mathcal{P}_8$. Thus, condition (b) holds. As a result, the objective value of problem $\mathcal{P}_0$ is non-increasing after each iteration of $\boldsymbol{Algorithm\ 1}$. This is the complete proof of the convergence of $\boldsymbol{Algorithm\ 1}$.

Within the $\boldsymbol{Algorithm\ 1}$, the joint active and passive beamforming problem in multiple vehicles scenario can be solved alternately. Due to the introduction of alternate iteration method in MVBA, the complexity of this algorithm is higher than that of SVBO method. According to [53], the complexity of the alternate optimization algorithm is $\mathcal{O}\left(\xi^{-1}\right)$, with ξ being iteration stop threshold. As for each iteration of the alternate optimization algorithm, the computational complexity is detailed as follows.

- SDP process: For a standard SDP problem, the complexity is determined by the number of variables. When optimizing the RIS parameters $\mathbf{\Omega}_t$ and $\mathbf{\Omega}_r$, the number of variables are N_{ts}^2 and N_{rs}^2, respectively, and the complexity are $\mathcal{O}\left(\left(N_{ts}^2+1\right)^{4.5}\right)$ and $\mathcal{O}\left(\left(N_{rs}^2+1\right)^{4.5}\right)$, respectively.
- GP process: The number of the variables for the GP problem is KN_t^2+1. The GP problem can be solved by using the interior point method, and the complexity can be expressed as $\mathcal{O}\left(\left(KN_t^2+1\right)^{3.5}\log\left(1/\Delta\right)\right)$, with the given solution accuracy Δ [54].

Consequentially, the total computational complexity of $\boldsymbol{Algorithm\ 1}$ is $\mathcal{O}(\xi^{-1}((N_{ts}^2+1)^{4.5}+(N_{ts}^2+1)^{4.5}+2(KN_t^2+1)^{3.5}\log(1/\Delta)))$. It is worth pointing out that a directional beam has a certain width in the far field, and the target vehicle is within the pointing range of the beam within a certain time slot. Therefore, we do not need to frequently adjust the direction of the beam in a short period of time, and the complexity of $\boldsymbol{Algorithm\ 1}$ can meet the needs of vehicle localization at each time slot.

VI. Numerical Rsults

In this section, we provide several examples to verify the performance of the proposed algorithms. The parameters in the experiments are designed as follows: the noise variance is $\sigma^2=0.005$, the carrier frequency is $f_c=3GHz$, the inter-element spacing of all antenna arrays is $d=0.05m$, the cosine exponent is $q=2$, and the sampling period is $N_T=100$. In addition, the Monte Carlo times in all simulation experiments is 1000.

A. The influence of different parameters in SVBO

In this subsection, we investigate the impact of SVBO on different variables, such as positioning accuracy, vehicle position and number of antenna arrays, etc. The optimal beam design is reflected by the total transmit power of the radar, as our goal is to minimize system resource overhead while meeting localization requirements by designing active and passive beamforming. In order to verify the relation between the transmit power and the vehicle position, we investigate the transmit power versus vehicle position under the different number of the RIS elements. We set the transmitter position as $\boldsymbol{p}_t=[0m,0m]^T$, the receiver position as $\boldsymbol{p}_r=[80m,0m]^T$, the two RISs' positions as $\boldsymbol{p}_{ts}=[-30m,30m]^T$ and $\boldsymbol{p}_{rs}=[110m,30m]^T$, respectively. The localization accuracy is set as $0.01m^2$, and the vertical coordinate position of the vehicle is set as $40m$. The vehicle position is adjusted by changing the horizontal coordinate position. The simulation results are shown in Fig. 2. The results imply that the transmit power requirement is minimal when the vehicle is located near the center position. However, it is worth emphasizing that the position with the lowest transmit power is slightly biased towards the direction of the transmitter, which is due to the benefits brought by the active beamforming of the transmitter. The curve results also show that the increase of RIS numbers can reduce the power demand of vehicle localization from the transmitter. It is reasonable that a larger RIS numbers results in greater freedom and antenna gain, and reduces the power overhead of transmitter.

We further discuss the impact of $\mathbf{RIS}_t$'s location deployment on the SVBO performance. Due to the RIS can construct virtual links through reflection, we set the vehicle target to the right of the transmitter and $\mathbf{RIS}_t$ to the left of the transmitter in our experiment. The vertical axis position of the $\mathbf{RIS}_t$

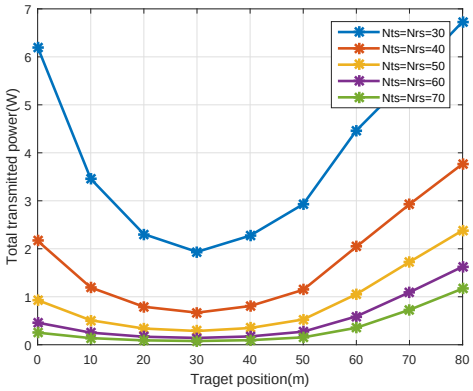

Fig. 2. Transmit power as a function of the vehicle position for SVBO in the case of the different number of the RISs' elements.

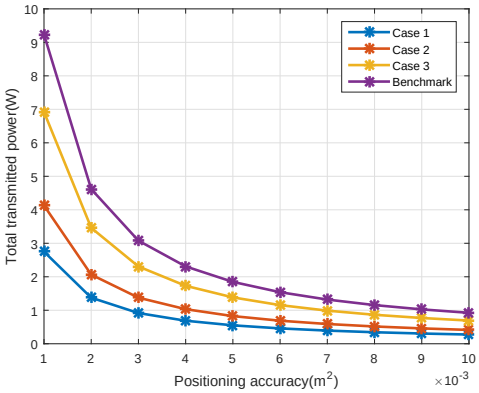

Fig. 4. Transmit power as a function of the localization accuracy for SVBO in the case of the different configurations.

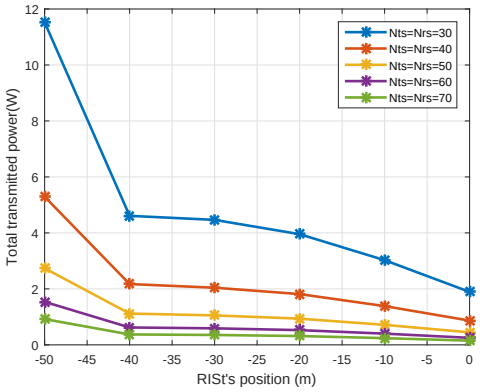

Fig. 3. Transmit power as a function of the $\mathbf{RIS}_t$'s position for SVBO in the case of the different number of the RISs' elements.

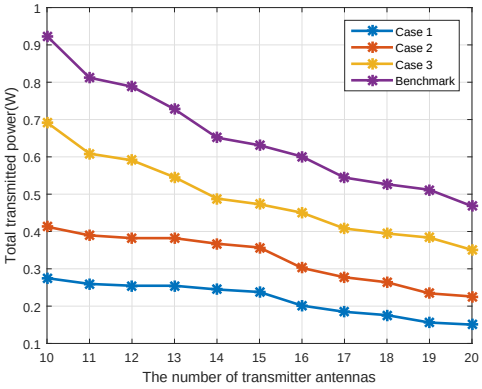

Fig. 5. Transmit power as a function of the number of transmitter antennas for SVBO in the case of the different configurations.

near the transmitter is fixed and its position is changed by adjusting its horizontal axis position. The results in Fig. 3 indicate that the distance between the transmitter and $\mathbf{RIS}_t$ affects the transmit power, and a significant trend jump point appears on the curve. This is because the distance at this point happens to be the Fresnel distance in this example. Thus, deploying $\mathbf{RIS}_t$ in the radar near-field area usually brings an effective improvement. When the distance between the transmitter and $\mathbf{RIS}_t$ achieves the smallest, we obtain the best system performance, where the spatial path loss is minimized.

In order to further illustrate the benefits that RIS brings to vehicle localization systems, we construct several comparative experiments to investigate the performance of the SVBO method. We report the total transmit power under different parameters by using two RISs, a RIS nearby transmitter only, and a RIS nearby receiver only, as compared to the case where the radar operates alone. The configurations considered here are as follows:

- $\mathbf{Case\ 1}$: $\mathbf{Transmitter\&RIS - Receiver\&RIS}$: the proposed complete RIS assisted vehicle localization system and utilizes the inference of Section IV to solve joint active and passive beamforming problem.
- $\mathbf{Case\ 2}$: $\mathbf{Transmitter\&RIS - Receiver}$: the RIS assisted vehicle localization system with a RIS nearby transmitter only, and the proposed method is applied to study the RIS gain near the transmitter.
- $\mathbf{Case\ 3}$: $\mathbf{Transmitter - Receiver\&RIS}$: the RIS assisted vehicle localization system with a RIS nearby receiver only, and the proposed method is applied to study the RIS gain near the receiver.
- $\mathbf{Benchmark}$: $\mathbf{Transmitter - Receiver}$: the vehicle localization system without any RIS. Applying the traditional method to solve the active beamforming results in this situation and serve as the benchmark for the proposed algorithm.

The results in Fig. 4 indicate the relationship between localization accuracy and transmit power under these configurations. The simulation indicates that the higher localization accuracy we set, the more transmit power is required from the transmitter. From the simulation results, it can be seen that there is a significant decline in the transmit power of transmitter with the assistance of RIS. The slightly lower transmit power of scenario "Case 2" compared to scenario "Case 3" is attributed to the active beamforming effect of the transmitter.

We further explore the impact of the number of transmitter antennas on transmit power. The simulation results in Fig. 5 show that the increase in the number of transmitter antennas is beneficial for reducing transmission power due to the

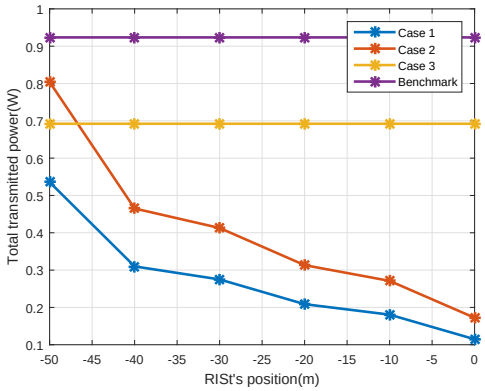

Fig. 6. Transmit power as a function of the $\mathbf{RIS}_t$'s position for SVBO in the case of the different configurations.

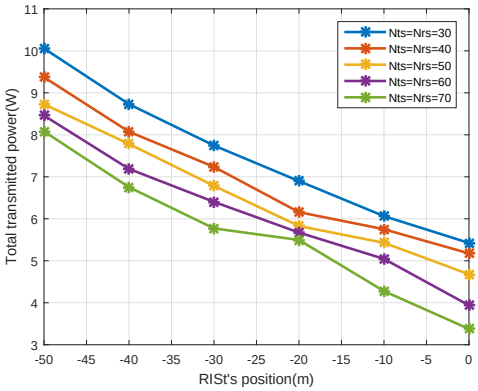

Fig. 8. Transmit power as a function of the $\mathbf{RIS}_t$'s position for MVBA in the case of the different number of the RISs' elements.

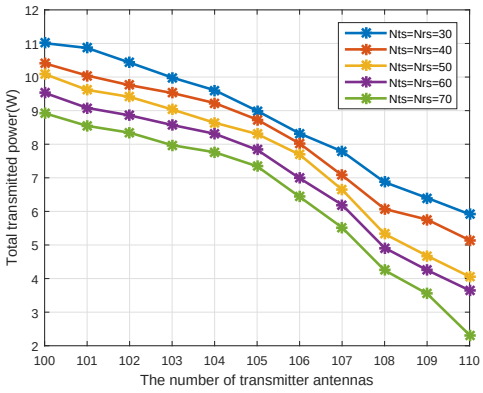

Fig. 7. Transmit power as a function of the number of transmitter antennas for MVBA in the case of the different number of the RISs' elements.

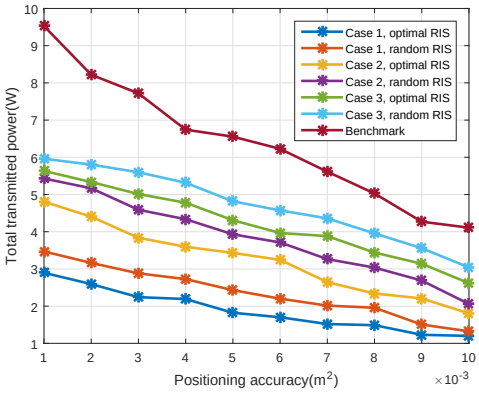

Fig. 9. Transmit power as a function of the localization accuracy for MVBA in the case of the different configurations.

higher antenna gain. Fig. 6 provides the impact of the RIS position nearby the transmitter on the performance of SVBO. The appearance of two straight lines in the curve is due to the absence of the RIS setting in these two configurations. Similarly, the curve results indicate that deploying RIS in the near field of the transmitter can provide better performance.

B. The influence of different parameters in MVBA

In this subsection, we investigate the effects of MVBA on different variables such as positioning accuracy, number of antennas, and $\mathbf{RIS}_t$'s position. We set the number of vehicles to 6 and randomly generate them within the region of interest. We provide Fig. 7 to verify the relationship between the transmit power and the number of transmitter antennas. We observe from the simulation results that the number of transmitter antennas affects the transmit power. We further discuss the impact of RIS location deployment on the MVBA performance. The vertical axis position of the RIS near the transmitter is fixed and its position is changed by adjusting its horizontal axis position. Based on the previous results, we only deploy the RIS within the near-field range of the transmitter. The results in Fig. 8 indicate that reducing the distance between the transmitter and RIS is beneficial for reducing transmission power. These simulation results reach consistent conclusions with SVBO.

We further provide some comparative experiments to illustrate the performance advantages of MVBA. The configurations considered here still correspond to the "Case 1", "Caes 2", "Caes 3" and "Benchmark" scenes. In addition, we also consider the comparison between optimal RIS and random RIS. The results in Figs. 9 and 10 provide the results of transmit power under localization accuracy and RIS position, respectively. From the simulation results, it can be concluded that the introduction and optimization of RIS have a significant improvement in the vehicle localization system. Finally, we validate the convergence of our proposed MVBA, as shown in Fig. 11. The graphical results show that our proposed algorithm converges after approximately 15 rounds of alternating iterations in our simulation environment, which proves the effectiveness of our algorithm.

VII. Conclusion

In this paper, we have investigated the joint active and passive beamforming problems for vehicle localization with RISs. In order to minimize the transmit power, we have presented two beamforming mothods of RIS-assisted vehicle localization under the constraints of the localization accuracy

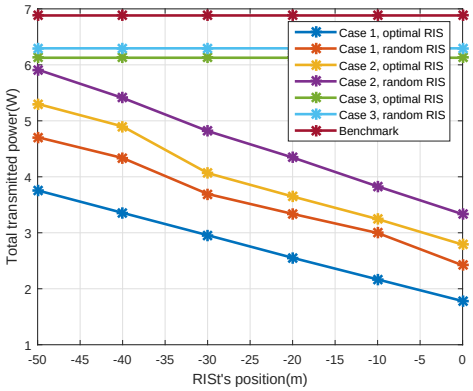

Fig. 10. Transmit power as a function of the $\mathbf{RIS}_t$'s position for MVBA in the case of the different configurations.

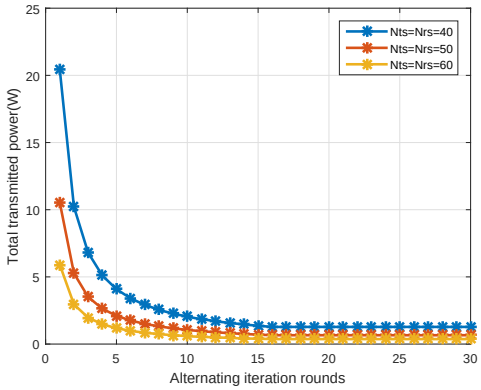

Fig. 11. Transmit power as a function of the alternating iteration rounds for MVBA in the case of the different number of the RISs' elements.

and the phase shift parameters of RIS. Specifically, we have derived the CRB of vehicle localization assisted by RISs as the performance metric, and have presented the closed form results of SVBO using the specialized form under this scenario. Subsequently, for the multiple vehicles scenario, we have decomposed the original non-convex optimal problem by using alternating iteration and obtained the SDP form using convex release to solve the passive beamforming problem. On this basis, the active beamforming problem have been transformed into a GP problem according to equivalent transformation and perspective function. The numerical results have been provided to verify the effectiveness of the presented methods.

APPENDIX A
DERIVATION OF FIM

According to formulas (12) and (13), the FIM $\boldsymbol{J}_{\eta_k}$ on the channel parameter $\boldsymbol{\eta}_k$ can be obtained as formula (14). The derivation of the FIM $\boldsymbol{J}_{\eta_k}$ is shown as follows:

$$\begin{aligned}\psi_{d_{t,k},d_{t,k}} = \frac{2}{\sigma^2}\sum\nolimits_{N_T}\omega_k^H\left(v_{t,k}\frac{\partial\gamma_{t,k}}{\partial d_{t,k}}+G_t\Omega_t\frac{\partial v_{ts,k}\gamma_{ts,k}}{\partial d_{t,k}}\right)\\ \left(v_{r,k}\gamma_{r,k}+G_r\Omega_r v_{rs,k}\gamma_{rs,k}\right)^H\\ \left(v_{r,k}\gamma_{r,k}+G_r\Omega_r v_{rs,k}\gamma_{rs,k}\right)\\ \left(\frac{\partial\gamma_{t,k}^*}{\partial d_{t,k}}v_{t,k}^H+\frac{\partial\gamma_{ts,k}^*v_{ts,k}^H}{\partial d_{t,k}}\Omega_t^HG_t^H\right)\omega_k,\end{aligned}\tag{47}$$

$$\begin{aligned}\psi_{d_{r,k},d_{r,k}} = \frac{2}{\sigma^2}\sum\nolimits_{N_T}\omega_k^H\left(v_{t,k}\gamma_{t,k}+G_t\Omega_t v_{ts,k}\gamma_{ts,k}\right)\\ \left(\frac{\partial\gamma_{r,k}^*}{\partial d_{r,k}}v_{r,k}^H+\frac{\partial\gamma_{rs,k}^*v_{rs,k}^H}{\partial d_{r,k}}\Omega_r^HG_r^H\right)\\ \left(v_{r,k}\frac{\partial\gamma_{r,k}}{\partial d_{r,k}}+G_r\Omega_r\frac{\partial v_{rs,k}\gamma_{rs,k}}{\partial d_{r,k}}\right)\\ \left(v_{t,k}\gamma_{t,k}+G_t\Omega_t v_{ts,k}\gamma_{ts,k}\right)^H\omega_k,\end{aligned}\tag{48}$$

$$\begin{aligned}\psi_{\theta_{t,k},\theta_{t,k}} = \frac{2}{\sigma^2}\sum\nolimits_{N_T}\omega_k^H\left(\frac{\partial v_{t,k}}{\partial\theta_{t,k}}\gamma_{t,k}+G_t\Omega_t\frac{\partial v_{ts,k}\gamma_{ts,k}}{\partial\theta_{t,k}}\right)\\ \left(v_{r,k}\gamma_{r,k}+G_r\Omega_r v_{rs,k}\gamma_{rs,k}\right)^H\\ \left(v_{r,k}\gamma_{r,k}+G_r\Omega_r v_{rs,k}\gamma_{rs,k}\right)\\ \left(\gamma_{t,k}^*\frac{\partial v_{t,k}^H}{\partial\theta_{t,k}}+\frac{\partial\gamma_{ts,k}^*v_{ts,k}^H}{\partial\theta_{t,k}}\Omega_t^HG_t^H\right)\omega_k,\end{aligned}\tag{49}$$

$$\begin{aligned}\psi_{\theta_{r,k},\theta_{r,k}} = \frac{2}{\sigma^2}\sum\nolimits_{N_T}\omega_k^H\left(v_{t,k}\gamma_{t,k}+G_t\Omega_t v_{ts,k}\gamma_{ts,k}\right)\\ \left(\gamma_{r,k}^*\frac{\partial v_{r,k}^H}{\partial\theta_{r,k}}+\frac{\partial\gamma_{rs,k}^*v_{rs,k}^H}{\partial\theta_{r,k}}\Omega_r^HG_r^H\right)\\ \left(\frac{\partial v_{r,k}}{\partial\theta_{r,k}}\gamma_{r,k}+G_r\Omega_r\frac{\partial v_{rs,k}\gamma_{rs,k}}{\partial\theta_{r,k}}\right)\\ \left(v_{t,k}\gamma_{t,k}+G_t\Omega_t v_{ts,k}\gamma_{ts,k}\right)^H\omega_k,\end{aligned}\tag{50}$$

$$\begin{aligned}\psi_{d_{t,k},d_{r,k}} = \frac{2}{\sigma^2}\sum\nolimits_{N_T}\omega_k^H\left(v_{t,k}\frac{\partial\gamma_{t,k}}{\partial d_{t,k}}+G_t\Omega_t\frac{\partial v_{ts,k}\gamma_{ts,k}}{\partial d_{t,k}}\right)\\ \left(v_{r,k}\gamma_{r,k}+G_r\Omega_r v_{rs,k}\gamma_{rs,k}\right)^H\\ \left(v_{r,k}\frac{\partial\gamma_{r,k}}{\partial d_{r,k}}+G_r\Omega_r\frac{\partial v_{rs,k}\gamma_{rs,k}}{\partial d_{r,k}}\right)\\ \left(v_{t,k}\gamma_{t,k}+G_t\Omega_t v_{ts,k}\gamma_{ts,k}\right)^H\omega_k,\end{aligned}\tag{51}$$

$$\begin{aligned}\psi_{\theta_{t,k},\theta_{r,k}} = \frac{2}{\sigma^2}\sum\nolimits_{N_T}\omega_k^H\left(\frac{\partial v_{t,k}}{\partial\theta_{t,k}}\gamma_{t,k}+G_t\Omega_t\frac{\partial v_{ts,k}\gamma_{ts,k}}{\partial\theta_{t,k}}\right)\\ \left(v_{r,k}\gamma_{r,k}+G_r\Omega_r v_{rs,k}\gamma_{rs,k}\right)^H\\ \left(\frac{\partial v_{r,k}}{\partial\theta_{r,k}}\gamma_{r,k}+G_r\Omega_r\frac{\partial v_{rs,k}\gamma_{rs,k}}{\partial\theta_{r,k}}\right)\\ \left(v_{t,k}\gamma_{t,k}+G_t\Omega_t v_{ts,k}\gamma_{ts,k}\right)^H\omega_k,\end{aligned}\tag{52}$$

$$\begin{aligned}\psi_{d_{t,k},\theta_{t,k}} = \frac{2}{\sigma^2}\sum\nolimits_{N_T}\omega_k^H\left(v_{t,k}\frac{\partial\gamma_{t,k}}{\partial d_{t,k}}+G_t\Omega_t\frac{\partial v_{ts,k}\gamma_{ts,k}}{\partial d_{t,k}}\right)\\ \left(v_{r,k}\gamma_{r,k}+G_r\Omega_r v_{rs,k}\gamma_{rs,k}\right)^H\\ \left(v_{r,k}\gamma_{r,k}+G_r\Omega_r v_{rs,k}\gamma_{rs,k}\right)\\ \left(\gamma_{t,k}^*\frac{\partial v_{t,k}^H}{\partial\theta_{t,k}}+\frac{\partial\gamma_{ts,k}^*v_{ts,k}^H}{\partial\theta_{t,k}}\Omega_t^HG_t^H\right)\omega_k,\end{aligned}\tag{53}$$

$$\begin{aligned}\psi_{d_{t,k},\theta_{r,k}} = \frac{2}{\sigma^2}\sum\nolimits_{N_T}\omega_k^H\left(v_{t,k}\frac{\partial\gamma_{t,k}}{\partial d_{t,k}}+G_t\Omega_t\frac{\partial v_{ts,k}\gamma_{ts,k}}{\partial d_{t,k}}\right)\\ \left(v_{r,k}\gamma_{r,k}+G_r\Omega_r v_{rs,k}\gamma_{rs,k}\right)^H\\ \left(\frac{\partial v_{r,k}}{\partial\theta_{r,k}}\gamma_{r,k}+G_r\Omega_r\frac{\partial v_{rs,k}\gamma_{rs,k}}{\partial\theta_{r,k}}\right)\\ \left(v_{t,k}\gamma_{t,k}+G_t\Omega_t v_{ts,k}\gamma_{ts,k}\right)^H\omega_k,\end{aligned}\tag{54}$$

$$\begin{aligned}\psi_{d_{r,k},\theta_{t,k}} = \frac{2}{\sigma^2}\sum\nolimits_{N_T}\omega_k^H\left(v_{t,k}\gamma_{t,k}+G_t\Omega_t v_{ts,k}\gamma_{ts,k}\right)\\ \left(\frac{\partial\gamma_{r,k}^*}{\partial d_{r,k}}v_{r,k}^H+\frac{\partial\gamma_{rs,k}^*v_{rs,k}^H}{\partial d_{r,k}}\Omega_r^HG_r^H\right)\\ \left(v_{r,k}\gamma_{r,k}+G_r\Omega_r v_{rs,k}\gamma_{rs,k}\right)\\ \left(\gamma_{t,k}^*\frac{\partial v_{t,k}^H}{\partial\theta_{t,k}}+\frac{\partial\gamma_{ts,k}^*v_{ts,k}^H}{\partial\theta_{t,k}}\Omega_t^HG_t^H\right)\omega_k,\end{aligned}\tag{55}$$

$$\begin{aligned}\psi_{d_{r,k},\theta_{r,k}} = \frac{2}{\sigma^2}\sum\nolimits_{N_T}\omega_k^H\left(v_{t,k}\gamma_{t,k}+G_t\Omega_t v_{ts,k}\gamma_{ts,k}\right)\\ \left(\frac{\partial\gamma_{r,k}^*}{\partial d_{r,k}}v_{r,k}^H+\frac{\partial\gamma_{rs,k}^*v_{rs,k}^H}{\partial d_{r,k}}\Omega_r^H G_r^H\right)\\ \left(\frac{\partial v_{r,k}}{\partial\theta_{r,k}}\gamma_{r,k}+G_r\Omega_r\frac{\partial v_{rs,k}\gamma_{rs,k}}{\partial\theta_{r,k}}\right)\\ \left(v_{t,k}\gamma_{t,k}+G_t\Omega_t v_{ts,k}\gamma_{ts,k}\right)^H\omega_k,\end{aligned} \tag{56}$$

where $\frac{\partial\gamma_{t,k}}{\partial d_{t,k}}$, $\frac{\partial\gamma_{r,k}}{\partial d_{r,k}}$, $\frac{\partial v_{t,k}}{\partial\theta_{t,k}}$ and $\frac{\partial v_{r,k}}{\partial\theta_{r,k}}$ are the one-step derivatives of direct parameter vector $\boldsymbol{\eta}_k = [d_{t,k}, d_{r,k}, \theta_{t,k}, \theta_{r,k}]^T$ for vehicle localization. Then, the result of composite derivative $\frac{\partial\gamma_{ts,k}v_{ts,k}}{\partial d_{t,k}}$, $\frac{\partial\gamma_{rs,k}v_{rs,k}}{\partial d_{r,k}}$, $\frac{\partial\gamma_{ts,k}v_{ts,k}}{\partial\theta_{t,k}}$ and $\frac{\partial\gamma_{rs,k}v_{rs,k}}{\partial\theta_{r,k}}$ can be represented as

$$\begin{aligned}\frac{\partial\gamma_{ts,k}v_{ts,k}}{\partial d_{t,k}} =& \frac{\partial\gamma_{ts,k}}{\partial d_{t,k}}v_{ts,k}+\gamma_{ts,k}\frac{\partial v_{ts,k}}{\partial d_{t,k}}\\ =&\left(\frac{\partial\gamma_{ts,k}}{\partial\varsigma_{t,k}}\frac{\partial\varsigma_{t,k}}{\partial\theta_{ts,k}}\frac{\partial\theta_{ts,k}}{\partial d_{t,k}}+\frac{\partial\gamma_{ts,k}}{\partial d_{ts,k}}\frac{\partial d_{ts,k}}{\partial d_{t,k}}\right)v_{ts,k}\\ &+\gamma_{ts,k}\frac{\partial v_{ts,k}}{\partial d_{ts,k}}\frac{\partial d_{ts,k}}{\partial d_{t,k}},\end{aligned} \tag{57}$$

$$\begin{aligned}\frac{\partial\gamma_{rs,k}v_{rs,k}}{\partial d_{r,k}} =& \frac{\partial\gamma_{rs,k}}{\partial d_{r,k}}v_{rs,k}+\gamma_{rs,k}\frac{\partial v_{rs,k}}{\partial d_{r,k}}\\ =&\left(\frac{\partial\gamma_{rs,k}}{\partial\varsigma_{r,k}}\frac{\partial\varsigma_{r,k}}{\partial\theta_{rs,k}}\frac{\partial\theta_{rs,k}}{\partial d_{r,k}}+\frac{\partial\gamma_{rs,k}}{\partial d_{rs,k}}\frac{\partial d_{rs,k}}{\partial d_{r,k}}\right)v_{rs,k}\\ &+\gamma_{ts,k}\frac{\partial v_{rs,k}}{\partial d_{rs,k}}\frac{\partial d_{rs,k}}{\partial d_{r,k}},\end{aligned} \tag{58}$$

$$\begin{aligned}\frac{\partial\gamma_{ts,k}v_{ts,k}}{\partial\theta_{t,k}} =& \frac{\partial\gamma_{ts,k}}{\partial\theta_{t,k}}v_{ts,k}+\gamma_{ts,k}\frac{\partial v_{ts,k}}{\partial\theta_{t,k}}\\ =&\left(\frac{\partial\gamma_{ts,k}}{\partial\varsigma_{t,k}}\frac{\partial\varsigma_{t,k}}{\partial\theta_{ts,k}}\frac{\partial\theta_{ts,k}}{\partial\theta_{t,k}}+\frac{\partial\gamma_{ts,k}}{\partial d_{ts,k}}\frac{\partial d_{ts,k}}{\partial\theta_{t,k}}\right)v_{ts,k}\\ &+\gamma_{ts,k}\frac{\partial v_{ts,k}}{\partial d_{ts,k}}\frac{\partial d_{ts,k}}{\partial\theta_{t,k}},\end{aligned} \tag{59}$$

$$\begin{aligned}\frac{\partial\gamma_{rs,k}v_{rs,k}}{\partial\theta_{r,k}} =& \frac{\partial\gamma_{rs,k}}{\partial\theta_{r,k}}v_{rs,k}+\gamma_{rs,k}\frac{\partial v_{rs,k}}{\partial\theta_{r,k}}\\ =&\left(\frac{\partial\gamma_{rs,k}}{\partial\varsigma_{r,k}}\frac{\partial\varsigma_{r,k}}{\partial\theta_{rs,k}}\frac{\partial\theta_{rs,k}}{\partial\theta_{r,k}}+\frac{\partial\gamma_{rs,k}}{\partial d_{rs,k}}\frac{\partial d_{rs,k}}{\partial\theta_{r,k}}\right)v_{rs,k}\\ &+\gamma_{ts,k}\frac{\partial v_{rs,k}}{\partial d_{rs,k}}\frac{\partial d_{rs,k}}{\partial\theta_{r,k}},\end{aligned} \tag{60}$$

where the one-step derivative results regarding indirect parameters are not expanded here. Meanwhile, the derivative relationship between RIS path parameters and direct path parameters can be written as

$$\frac{\partial d_{ts,k}}{\partial d_{t,k}} = \frac{d_{t,k}+\delta_{ts}\cos\left(\theta_{t,k}+\rho_{ts}\right)}{\sqrt{\delta_{ts}^2+d_{t,k}^2+2\delta_{ts}d_{t,k}\cos\left(\theta_{t,k}+\rho_{ts}\right)}}, \tag{61}$$

$$\frac{\partial d_{rs,k}}{\partial d_{r,k}} = \frac{d_{r,k}+\delta_{rs}\cos\left(\theta_{r,k}+\rho_{rs}\right)}{\sqrt{\delta_{rs}^2+d_{r,k}^2+2\delta_{rs}d_{r,k}\cos\left(\theta_{r,k}+\rho_{rs}\right)}}, \tag{62}$$

$$\frac{\partial\theta_{ts,k}}{\partial d_{t,k}} = \frac{\frac{\delta_{ts}\left(\sin\theta_{t,k}\cos\rho_{ts}-\cos\theta_{t,k}\sin\rho_{ts}\right)}{\left(d_{t,k}\cos\theta_{t,k}+\delta_{ts}\cos\rho_{ts}\right)^2}}{1+\left(\frac{d_{t,k}\sin\theta_{t,k}-\delta_{ts}\sin\rho_{ts}}{d_{t,k}\cos\theta_{t,k}+\delta_{ts}\cos\rho_{ts}}\right)^2}, \tag{63}$$

$$\frac{\partial\theta_{rs,k}}{\partial d_{r,k}} = \frac{\frac{\delta_{rs}\left(\sin\theta_{r,k}\cos\rho_{rs}-\cos\theta_{r,k}\sin\rho_{rs}\right)}{\left(d_{r,k}\cos\theta_{r,k}+\delta_{rs}\cos\rho_{rs}\right)^2}}{1+\left(\frac{d_{r,k}\sin\theta_{r,k}-\delta_{rs}\sin\rho_{rs}}{d_{r,k}\cos\theta_{r,k}+\delta_{rs}\cos\rho_{rs}}\right)^2}, \tag{64}$$

$$\frac{\partial d_{ts,k}}{\partial\theta_{t,k}} = \frac{-\delta_{ts}d_{t,k}\sin\left(\theta_{t,k}+\rho_{ts}\right)}{\sqrt{\delta_{ts}^2+d_{t,k}^2+2\delta_{ts}d_{t,k}\cos\left(\theta_{t,k}+\rho_{ts}\right)}}, \tag{65}$$

$$\frac{\partial d_{rs,k}}{\partial\theta_{r,k}} = \frac{-\delta_{rs}d_{r,k}\sin\left(\theta_{r,k}+\rho_{rs}\right)}{\sqrt{\delta_{rs}^2+d_{r,k}^2+2\delta_{rs}d_{r,k}\cos\left(\theta_{r,k}+\rho_{rs}\right)}}, \tag{66}$$

$$\frac{\partial\theta_{ts,k}}{\partial\theta_{t,k}} = \frac{\frac{d_{t,k}^2+\delta_{ts}d_{t,k}\left(\cos\theta_{t,k}\cos\rho_{ts}+\sin\theta_{t,k}\sin\rho_{ts}\right)}{\left(d_{t,k}\cos\theta_{t,k}+\delta_{ts}\cos\rho_{ts}\right)^2}}{1+\left(\frac{d_{t,k}\sin\theta_{t,k}-\delta_{ts}\sin\rho_{ts}}{d_{t,k}\cos\theta_{t,k}+\delta_{ts}\cos\rho_{ts}}\right)^2}, \tag{67}$$

$$\frac{\partial\theta_{rs,k}}{\partial\theta_{r,k}} = \frac{\frac{d_{r,k}^2+\delta_{rs}d_{r,k}\left(\cos\theta_{r,k}\cos\rho_{rs}+\sin\theta_{r,k}\sin\rho_{rs}\right)}{\left(d_{r,k}\cos\theta_{r,k}+\delta_{rs}\cos\rho_{rs}\right)^2}}{1+\left(\frac{d_{r,k}\sin\theta_{r,k}-\delta_{rs}\sin\rho_{rs}}{d_{r,k}\cos\theta_{r,k}+\delta_{rs}\cos\rho_{rs}}\right)^2}. \tag{68}$$

APPENDIX B
PROOF OF PROPOSITION 2

The Lagrange function of the problem $\mathcal{P}_3$ can be written as

$$L\left(\boldsymbol{W}_1,\lambda\right) = tr\left(\boldsymbol{W}_1\right)-\lambda\left(tr\left(\boldsymbol{H}_{t,1}\boldsymbol{W}_1\right)-\frac{\sigma^2}{2N_T\left\|\dot{\boldsymbol{h}}_{r,1}\right\|^2\varepsilon_1}\right), \tag{69}$$

where $\lambda \geq 0$ is the Lagrange inequality multiplier. The Lagrange dual function can be expressed as

$$g\left(\lambda\right) = \inf_{\boldsymbol{W}_1\succeq 0} L\left(\boldsymbol{W}_1,\lambda\right). \tag{70}$$

The corresponding Lagrange dual problem can be represented as

$$\max_{\lambda\geq 0}\ \ g\left(\lambda\right). \tag{71}$$

Obviously, this dual problem has strong duality. So the dual problem has the same optimal value as the original problem. Suppose λ^* is the optimal solution of the dual problem, then the $\boldsymbol{W}_1^*$ satisfying $\inf_{\boldsymbol{W}_1\succeq 0} L\left(\boldsymbol{W}_1,\lambda^*\right)$ is the optimal solution of problem $\mathcal{P}_3$. Therefore, we can find $\boldsymbol{W}_1^*$ through the following optimization problem

$$\min_{\boldsymbol{W}_1\succeq 0}\ \ tr\left(\boldsymbol{W}_1\right)-tr\left(\lambda^*\boldsymbol{H}_{t,1}\boldsymbol{W}_1\right). \tag{72}$$

$\lambda^*\boldsymbol{H}_{t,1}$ is positive semidefinite, and we define $\boldsymbol{Q} = \lambda^*\boldsymbol{H}_{t,1}$. Let $\bar{\boldsymbol{W}}_1 = \boldsymbol{Q}^{1/2}\boldsymbol{W}_1\boldsymbol{Q}^{1/2}$, then this problem can be rewritten as

$$\min_{\bar{\boldsymbol{W}}_1\succeq 0}\ \ \left(\boldsymbol{Q}^{-1/2}\mathbf{1}\right)^H\bar{\boldsymbol{W}}_1\left(\boldsymbol{Q}^{-1/2}\mathbf{1}\right)-tr\left(\bar{\boldsymbol{W}}_1\right). \tag{73}$$

Then we can conclude that the optimal solution $\bar{\boldsymbol{W}}_1^*$ satisfies $rank\left(\bar{\boldsymbol{W}}_1^*\right) = 1$. Assume that $rank\left(\bar{\boldsymbol{W}}_1^*\right) \neq 1$, that is,

$rank\left(\bar{\boldsymbol{W}}_1^*\right)=k, 2\leq k\leq N_t$. Through eigenvalue decomposition, we obtain $\bar{\boldsymbol{W}}_1^*=\sum_{j=1}^{k}\alpha_j\bar{\boldsymbol{\omega}}_j\bar{\boldsymbol{\omega}}_j^H$. At present, we can find a solution that satisfies $\bar{\boldsymbol{W}}_1'=\left(\sum_{j=1}^{k}\alpha_j\right)\bar{\boldsymbol{\omega}}_i\bar{\boldsymbol{\omega}}_i^H$, where $i=\arg\min_{j\in\{1,2,\cdots,k\}}\left|\left(\boldsymbol{Q}^{-1/2}\mathbf{1}\right)^H\bar{\boldsymbol{\omega}}_j\right|$ making the problem obtain a smaller optimal value, which means that the assumption does not hold. So $rank\left(\bar{\boldsymbol{W}}_1^*\right)=1$. Because of $\boldsymbol{W}_1^*=\boldsymbol{Q}^{-1/2}\bar{\boldsymbol{W}}_1^*\boldsymbol{Q}^{-1/2}$, we can obtain $rank\left(\boldsymbol{W}_1^*\right)=1$.

REFERENCES

[1] A. T. Nguyen, J. Rath, T. M. Guerra, R. Palhares and H. Zhang, "Robust Set-Invariance Based Fuzzy Output Tracking Control for Vehicle Autonomous Driving Under Uncertain Lateral Forces and Steering Constraints," *IEEE Transactions on Intelligent Transportation Systems*, vol. 22, no. 9, pp. 5849-5860, Sept. 2021.

[2] S. Xu and H. Peng, "Design, Analysis, and Experiments of Preview Path Tracking Control for Autonomous Vehicles," *IEEE Transactions on Intelligent Transportation Systems*, vol. 21, no. 1, pp. 48-58, Jan. 2020.

[3] Q. Zou, H. Ling, Y. Pang, Y. Huang and M. Tian, "Joint Headlight Pairing and Vehicle Tracking by Weighted Set Packing in Nighttime Traffic Videos," *IEEE Transactions on Intelligent Transportation Systems*, vol. 19, no. 6, pp. 1950-1961, Jun. 2018.

[4] Y. Zhou, T. Wang, R. Hu, H. Su, Y. Liu, X. Liu, J. Suo and H. Snoussi, "Multiple Kernelized Correlation Filters (MKCF) for Extended Object Tracking Using X-Band Marine Radar Data," *IEEE Transactions on Signal Processing*, vol. 67, no. 14, pp. 3676-3688, 15 Jul., 2019.

[5] S. P. Ebenezer and A. Papandreou-Suppappola, "Generalized Recursive Track-Before-Detect With Proposal Partitioning for Tracking Varying Number of Multiple Targets in Low SNR," *IEEE Transactions on Signal Processing*, vol. 64, no. 11, pp. 2819-2834, Jun., 2016.

[6] Z. Yu, J. Li and Q. Guo, "Message Passing Based Target Localization Under Range Deception Jamming in Distributed MIMO Radar," *IEEE Signal Processing Letters*, vol. 28, pp. 1858-1862, Aug. 2021.

[7] Z. Zheng, M. Fu, W. -Q. Wang and H. C. So, "Symmetric Displaced Coprime Array Configurations for Mixed Near- and Far-Field Source Localization," *IEEE Transactions on Antennas and Propagation*, vol. 69, no. 1, pp. 465-477, Jan. 2021.

[8] S. A. R. Kazemi, R. Amiri and F. Behnia, "Efficient Convex Solution for 3-D Localization in MIMO Radars Using Delay and Angle Measurements," *IEEE Communications Letters*, vol. 23, no. 12, pp. 2219-2223, Dec. 2019.

[9] X. Zhao, J. Li and Q. Guo, "A Relaxed Energy Function Based Analog Neural Network Approach to Target Localization in Distributed MIMO Radar," *IEEE Transactions on Vehicular Technology*, vol. 71, no. 10, pp. 11160-11173, Oct. 2022.

[10] L. Zhu, G. Wen and Y. Liang, "Performance Boosting for Two-Step Localization Methods in Distributed MIMO Radar via a Robust Post-Processing Scheme," *IEEE Communications Letters*, vol. 27, no. 2, pp. 536-540, Feb. 2023.

[11] K. Zhu, Y. Wei and R. Xu, "TOA-based Localization Error Modeling of Distributed MIMO Radar for Positioning Accuracy Enhancement," *2016 CIE International Conference on Radar (RADAR)*, Guangzhou, China, pp. 1-5, Oct. 2016.

[12] Y. Feng, G. Zeng, Y. Jiang and H. Fan, "Positioning Error Analysis of Frequency-division Orthogonal MIMO Radar by TDOA Positioning System," *2022 4th International Conference on Frontiers Technology of Information and Computer (ICFTIC)*, Qingdao, China, pp. 592-598, Dec. 2022.

[13] B. Li, S. Wang, J. Zhang, X. Cao and C. Zhao, "Ultra-Fast Accurate AoA Estimation via Automotive Massive-MIMO Radar," *IEEE Transactions on Vehicular Technology*, vol. 71, no. 2, pp. 1172-1186, Feb. 2022.

[14] R. Amiri, F. Behnia and H. Zamani, "Efficient 3-D Positioning Using Time-Delay and AOA Measurements in MIMO Radar Systems," *IEEE Communications Letters*, vol. 21, no. 12, pp. 2614-2617, Dec. 2017.

[15] M. -M. Liu, W. Gao and Y. Zhao, "An Efficient Estimator for Source Localization Using TD and AOA Measurements in MIMO Radar Systems," *IEEE Sensors Letters*, vol. 5, no. 3, pp. 1-4, Mar. 2021.

[16] M. A. ElMossallamy, H. Zhang, L. Song, K. G. Seddik, Z. Han and G. Y. Li, "Reconfigurable Intelligent Surfaces for Wireless Communications: Principles, Challenges, and Opportunities," *IEEE Transactions on Cognitive Communications and Networking*, vol. 6, no. 3, pp. 990-1002, Sept. 2020.

[17] Ö. Özdogan, E. Bjornson and E. G. Larsson, "Intelligent Reflecting Surfaces: Physics, Propagation, and Pathloss Modeling," *IEEE Wireless Communications Letters*, vol. 9, no. 5, pp. 581-585, May 2020.

[18] S. Hu, F. Rusek and O. Edfors, "Beyond Massive MIMO: The Potential of Positioning With Large Intelligent Surfaces," *IEEE Transactions on Signal Processing*, vol. 66, no. 7, pp. 1761-1774, Apr. 2018.

[19] H. Zhang, J. Hu, H. Zhang, B. Di, K. Bian, Z. Han, and L. Song, "MetaRadar: Indoor Localization by Reconfigurable Metamaterials," *IEEE Transactions on Mobile Computing*, vol. 21, no. 8, pp. 2895-2908, Aug. 2022.

[20] J. He, H. Wymeersch, T. Sanguanpuak, O. Silven and M. Juntti, "Adaptive Beamforming Design for mmWave RIS-Aided Joint Localization and Communication," *2020 IEEE Wireless Communications and Networking Conference Workshops (WCNCW)*, Seoul, Korea (South), pp. 1-6, Jun. 2020.

[21] D. Dardari, N. Decarli, A. Guerra and F. Guidi, "LOS/NLOS Near-Field Localization With a Large Reconfigurable Intelligent Surface," *IEEE Transactions on Wireless Communications*, vol. 21, no. 6, pp. 4282-4294, Jun. 2022.

[22] Y. Huang, J. Yang, W. Tang, C. -K. Wen, S. Xia and S. Jin, "Joint Localization and Environment Sensing by Harnessing NLOS Components in RIS-aided mmWave Communication Systems," *IEEE Transactions on Wireless Communications*, Apr. 2023.

[23] M. Luan, B. Wang, Y. Zhao, Z. Feng and F. Hu, "Phase Design and Near-Field Target Localization for RIS-Assisted Regional Localization System," *IEEE Transactions on Vehicular Technology*, vol. 71, no. 2, pp. 1766-1777, Feb. 2022.

[24] H. Zhang, "Joint Waveform and Phase Shift Design for RIS-Assisted Integrated Sensing and Communication Based on Mutual Information," *IEEE Communications Letters*, vol. 26, no. 10, pp. 2317-2321, Oct. 2022.

[25] X. Tong, Z. Zhang, J. Wang, C. Huang and M. Debbah, "Joint Multi-User Communication and Sensing Exploiting Both Signal and Environment Sparsity," *IEEE Journal of Selected Topics in Signal Processing*, vol. 15, no. 6, pp. 1409-1422, Nov. 2021.

[26] X. Gan, C. Zhong, C. Huang and Z. Zhang, "RIS-Assisted Multi-User MISO Communications Exploiting Statistical CSI," *IEEE Transactions on Communications*, vol. 69, no. 10, pp. 6781-6792, Oct. 2021.

[27] X. Gan, C. Zhong, C. Huang, Z. Yang and Z. Zhang, "Multiple RISs Assisted Cell-Free Networks With Two-Timescale CSI: Performance Analysis and System Design," *IEEE Transactions on Communications*, vol. 70, no. 11, pp. 7696-7710, Nov. 2022.

[28] J. Zhou, H. Li and W. Cui, "Low-Complexity Joint Transmit and Receive Beamforming for MIMO Radar With Multi-Targets," *IEEE Signal Processing Letters*, vol. 27, pp. 1410-1414, Aug. 2020.

[29] J. Zhou, H. Li and W. Cui, "Joint Design of Transmit and Receive Beamforming for Transmit Subaperturing MIMO Radar," *IEEE Signal Processing Letters*, vol. 26, no. 11, pp. 1648-1652, Nov. 2019.

[30] L. Lan, G. Liao, J. Xu, Y. Zhang and B. Liao, "Transceive Beamforming With Accurate Nulling in FDA-MIMO Radar for Imaging," *IEEE Transactions on Geoscience and Remote Sensing*, vol. 58, no. 6, pp. 4145-4159, Jun. 2020.

[31] Y. Wang, D. Zhu, G. Jin, Q. Yu, P. Wang, S. Niu, Y. Cheng and D. Wu, "A Robust Digital Beamforming on Receive in Elevation for Airborne MIMO SAR System," *IEEE Transactions on Geoscience and Remote Sensing*, vol. 60, pp. 1-19, Aug. 2022.

[32] X. Liu, T. Huang, N. Shlezinger, Y. Liu, J. Zhou and Y. C. Eldar, "Joint Transmit Beamforming for Multiuser MIMO Communications and MIMO Radar," *IEEE Transactions on Signal Processing*, vol. 68, pp. 3929-3944, Jun. 2020.

[33] F. Wang, H. Li and J. Fang, "Joint Active and Passive Beamforming for IRS-Assisted Radar," *IEEE Signal Processing Letters*, vol. 29, pp. 349-353, Dec. 2021.

[34] S. Buzzi, E. Grossi, M. Lops and L. Venturino, "Foundations of MIMO Radar Detection Aided by Reconfigurable Intelligent Surfaces," *IEEE Transactions on Signal Processing*, vol. 70, pp. 1749-1763, Mar. 2022.

[35] S. Huang, B. Wang, Y. Zhao and M. Luan, "Near-Field RSS-Based Localization Algorithms Using Reconfigurable Intelligent Surface," *IEEE Sensors Journal*, vol. 22, no. 4, pp. 3493-3505, Feb. 2022.

[36] P. Mei, Y. Cai, K Zhao, Z. Ying, G. Pedersen, X. Lin and S. Zhang, "On the Study of Reconfigurable Intelligent Surfaces in the Near-Field Region," *IEEE Transactions on Antennas and Propagation*, vol. 70, no. 10, pp. 8718-8728, Oct. 2022.

[37] X. Zhang and H. Zhang, "Hybrid Reconfigurable Intelligent Surfaces-Assisted Near-Field Localization," *IEEE Communications Letters*, vol. 27, no. 1, pp. 135-139, Jan. 2023.

[38] H. Lu, Y. Zeng, S. Jin and R. Zhang, "Aerial Intelligent Reflecting Surface: Joint Placement and Passive Beamforming Design With 3D Beam Flattening," *IEEE Transactions on Wireless Communications*, vol. 20, no. 7, pp. 4128-4143, July 2021.

[39] Y. Jiang, H. Hu, S. Yang, J. Zhang and J. Zhang, "Generalized 3-D Spatial Scattering Modulation," *IEEE Transactions on Wireless Communications*, vol. 21, no. 3, pp. 1570-1585, March 2022.

[40] M. A. Richards, *Fundamentals of radar signal processing*, 2nd ed. New York, NY, USA: McGraw-Hill, 2005.

[41] C. P. Meyer and H. A. Mayer, *Radar target detection*. New York, NY, USA: Academic Press, 1973.

[42] V. Jamali, A. M. Tulino, G. Fischer, R. R. Mller, and R. Schober, "Intelligent Surface-aided Transmitter Architectures for Millimeter-wave Ultra Massive MIMO Systems," *IEEE Open Journal of the Communications Society*, vol. 2, pp. 144-167, Dec. 2020.

[43] M. Najafi, V. Jamali, R. Schober, and H. V. Poor, "Physics-based Modeling and Scalable Optimization of Large Intelligent Reflecting Surfaces," *IEEE Transactions on Communications*, vol. 69, no. 4, pp. 2673-2691, Apr. 2021.

[44] S. W. Ellingson, "Path Loss in Reconfigurable Intelligent Surfaceenabled Channels," *arXiv:1912.06759*, 2019. [Online]. Available: http://arxiv.org/abs/1912.06759.

[45] W. Tang, M. Chen, X. Chen, J. Dai, Y. Han, M. Renzo, Y. Zeng, S. Jin, Q. Cheng and T. Cui, "Wireless Communications with Reconfigurable Intelligent Surface: Path Loss Modeling and Experimental Measurement," *IEEE Transactions on Wireless Communications*, vol. 20, no. 1, pp. 421-439, Jan. 2021.

[46] A. Hassanien, M. W. Morency, A. Khabbazibasmenj, S. A. Vorobyov, J. Y. Park and S. J. Kim, "Two-dimensional Transmit Beamforming for MIMO Radar with Sparse Symmetric Arrays," *2013 IEEE Radar Conference (RadarCon13)*, pp. 1-6, 2013.

[47] S. M. Kay, *Fundamentals of statistical signal processing*, Estimation Theory. Englewood Cliffs, NJ, USA: Prentice Hall, 1998.

[48] I. Bekkerman and J. Tabrikian, "Target Detection and Localization using MIMO Radars and Sonars," *IEEE Transactions on Signal Processing*, vol. 54, no. 10, pp. 3873-3883, Oct. 2006.

[49] S. Boyd and L. Vandenberghe, *Convex Optimization*. Cambridge, U.K. Cambridge Univ. Press, 2004.

[50] N. Zhang, H. Song, J. Tang and Y. Shen, "Power Optimization for Joint Target Position and Velocity Estimation in MIMO Radar Networks," *2015 10th International Conference on Information, Communications and Signal Processing (ICICS)*, Singapore, 2015.

[51] M. Grant and S. Boyd, "CVX: MATLAB software for disciplined convex programming," 2014.

[52] Q. Wu and R. Zhang, "Intelligent Reflecting Surface Enhanced Wireless Network: Joint Active and Passive Beamforming Design," *2018 IEEE Global Communications Conference*, Abu Dhabi, United Arab Emirates, Dec. 2018.

[53] M. Hong, X. Wang, M. Razaviyayn, and Z.-Q. Luo, "Iteration complexity analysis of block coordinate descent methods," *Mathematical Programming*, vol. 163, no. 1-2, pp. 85-114, May 2017.

[54] Z. Q. Luo, W. K. Ma, A. M. C. So, Y. Ye, and S. Zhang, "Semidefinite Relaxation of Quadratic Optimization Problems," *IEEE Signal Processing Magazine*, vol. 27, no. 3, pp. 20-34, 2010.

Zhiyuan Feng (Graduate Student Member, IEEE) received the B.S. degree from the Electronic Information Engineering, North China Electric Power University, Beijing, China, in 2018. He is currently working toward the Ph.D. degree with the College of Communication and Engineering, Jilin University, Changchun, China. In 2022, he was a Visiting Ph.D. Student with the Faculty of Information Technology, University of Jyväskylä, Jyväskylä, Finland. His research interests include signal detection and estimation, deep reinforcement learning, and localization technology.

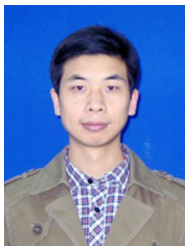

Bo Wang received the Ph.D. degree in communication and information systems from Jilin University, Changchun, China, in 2006. From July 2014 to July 2015, he was a Visiting Scholar with the Department of Electrical and Computer Engineering, Tennessee Technological University, Cookeville, TN, USA. He is currently a Professor with the College of Communication and Engineering, Jilin University. His research interests include graph signal processing, reconfigurable intelligent surface, resource allocation, signal detection, integrated sensing and communication, and source localization.

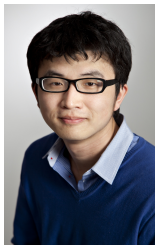

Zheng Chang (Senior Member, IEEE) received the B.Eng. degree from Jilin University, Changchun, China in 2007, M.Sc. (Tech.) degree from Helsinki University of Technology (Now Aalto University), Espoo, Finland in 2009 and Ph.D degree from the University of Jyväskylä, Jyväskylä, Finland in 2013. Since 2008, he has held various research positions at Helsinki University of Technology, University of Jyväskylä and Magister Solutions Ltd in Finland. He was a visiting researcher at Tsinghua University in 2013, and at University of Houston in 2015. He has been awarded by the Ulla Tuominen Foundation, the Nokia Foundation and the Riitta and Jorma J. Takanen Foundation for his research excellence. He has been awarded as 2018 IEEE Communications Society best young researcher for Europe, Middle East and Africa Region and 2021 IEEE Communications Society MMTC Outstanding Young Researcher. He has published over 150 papers in journals and conferences, and received best paper awards from IEEE TCGCC and APCC in 2017. He serves as an editor of IEEE Wireless Communications Letters, Springer Wireless Networks and International Journal of Distributed Sensor Networks, and a guest editor for IEEE Network, IEEE Wireless Communications, IEEE Communications Magazine, IEEE Internet of Things Journal, IEEE Transactions on Industrial Informatics, Physical Communications, and EURASIP Journal on Wireless Communications and Networking. He was the exemplary reviewer of IEEE Wireless Communication Letters in 2018. He has participated in organizing workshop and special session in Globecom' 19, WCNC'18-22, SPAWC'19 and ISWCS'18. He also serves as Symposium co-chair of IEEE ICC'20 and Globecom'23, Publicity co-chair of IEEE Infocom'22, Workshop co-chair of ICCC'22, TPC co-chair of IEEE iThing'22, and TPC member for many IEEE major conferences, such as INFOCOM, ICC, and Globecom. His research interests include IoT, cloud/edge computing, security and privacy, vehicular networks, and green communications.

Timo Hämäläinen (Senior Member, IEEE) has over 30 years¡¯ research and teaching experience of the computer networks and networking security. He has leaded tens of external funded network management related projects. He has launched and leaded Master Program in the University of Jyväskylä (Softwarwe&Commummincations Engineering) and teaches the network management and security related courses. He has more than 230 internationally peer reviewed publications and he has supervised over 40 Ph.D theses. Prof. Hämäläinen's research interests include currently network resource management, IoT, and networking security.

Yanping Zhao received the Ph.D. degree in communication and information systems from Jilin University, Changchun, China, in 2014. She is currently a Lecturer with the College of Communication Engineering, Jilin University. Her research interests include speech signal processing, resource allocation, wireless localization and sparse signal processing.

Fengye Hu (Senior Member, IEEE) received the B.S. degree from the Department of Precision Instrument, Xi'an University of Technology, Xi'an, China, in 1996, and the M.S. and Ph.D. degrees in communication and information systems from Jilin University, Changchun, China, in 2000 and 2007, respectively. In 2011, he was a Visiting Scholar in electrical and electronic engineering with Nanyang Technological University (NTU), Singapore. He is currently a Full Professor with the College of Communication Engineering, Jilin University. He has authored or coauthored 50 publications in IEEE journals and conferences. His current research interests include wireless body area networks, wireless energy and information transfer, energy harvesting, cognitive radio, and space-time communication. He is the Editor of IET Communications and China Communications, and the Editor of Physical Communication on special issue on ultra-reliable, low-latency and low-power transmissions in the era of Internet-of-Things. He organized the first and second Asia-Pacific Workshop on Wireless Networking and Communications (APWNC 2013 and APWNC 2015). He also organized the Future 5G Forum on Wireless Communications and Networking Big Data (FWCN 2016). He is an Editor of *IET Communications and China Communications and Physical Communication* on Special Issue on Ultra-Reliable, Low-Latency, and Low-Power Transmissions in the era of Internet-of-Things.